Modelling CO_2 dispersion in the air during potential limnic eruption at the lake Pavin (France)

V. Rafflin [a,1,*], G. Boudoire [a,b,*,1], S. Massaro [c,d], M. Stocchi [d,2], A. Costa [d], F. Grassa [b], G. Giuffrida [e], L. Gailler [a], M. Liuzzo [b,f], C. Planche [g,h], S. Banson [g], A. Harris [a]

[a] Université Clermont Auvergne, CNRS, IRD, OPGC, Laboratoire Magmas et Volcans (LMV), F-63000 Clermont-Ferrand, France
[b] Istituto Nazionale di Geofisica e Vulcanologia (INGV), Sezione di Palermo, 90146 Palermo, Italy
[c] Dipartimento di Scienze della Terra e Geoambientali, Università di Bari, 70125 Bari, Italy
[d] Istituto Nazionale di Geofisica e Vulcanologia (INGV), Sezione di Bologna, 40126 Bologna, Italy
[e] Istituto Nazionale di Geofisica e Vulcanologia (INGV), Sezione di Catania, 95125 Catania, Italy
[f] Department of Physics and Earth Sciences, University of Ferrara, Via Saragat 1, 44121 Ferrara, Italy
[g] Université Clermont Auvergne, CNRS, Laboratoire de Météorologie Physique (LaMP), 63000 Clermont-Ferrand, France
[h] Institut Universitaire de France (IUF), France

ARTICLE INFO

ABSTRACT

Risk mitigation in long-dormant volcanic provinces is a challenge due to the absence of collective memory of past disasters as well as the scarcity, and subtlety, of unrest signals that can be monitored. In this study, the impact of a potential limnic eruption is assessed at the 92-m-deep lake Pavin (French Massif Central). The lake is hosted in a maar crater formed during the last eruptive event in metropolitan France (~7 ka) and contains dissolved CO_2 in the deepest water layer, below 60 m. Carbon dioxide (CO_2) emissions measured at the lake surface (0.44 km^2) reach up to 10.1 tons/day during the winter. Beyond this (limited) continuous degassing of the lake, the current CO_2 budget in the monimolimnion layer (at a depth of 60 m to 92 m) was estimated at 1750 tons, of which about 450 tons are available for release in case of overturn of the lake. Scenarios for CO_2 dispersion in the lower atmosphere were simulated with the DISGAS and TWODEE-2 models by varying (i) meteorological conditions, (ii) the amount of CO_2 released, (iii) and the mechanisms of degassing during a potential limnic eruption. The simulations allowed identification and delimitation of areas potentially impacted by hazardous CO_2 levels in the air down-valley from the lake and directly around the lake. The spatio-temporal evolution of the potential CO_2 cloud raises issues regarding the impacts of such a hypothetical event in the close vicinity of the lake and, given the area is populated and highly visited, needs to be considered in future risk mitigation strategies.

1. Introduction

The long quiescent phase of some volcanic provinces tends to favour the settlement of local populations and economic activities in potentially hazardous areas. Indeed, almost one in eight people live within 100 km of a volcano (Brown et al., 2015; Small and Naumann, 2001). In long-dormant volcanic provinces, risk mitigation is a challenge due to (1) the absence of collective memory of past disasters, (2) the scarcity of, and subtlety, of unrest signals, that may be monitored, (3) absence of past forecasted eruptive events, and/or, (4) a lack of strategies for risk mitigation. In such cases, outgassing events (soil degassing, fumarolic emissions, bubbling spring waters, dissolved gases in water) are often the only manifestations of a residual magmatic and/or hydrothermal activity (Battani et al., 2010; Gal et al., 2011, 2018). They are, though, associated with a potentially eruptive system that poses a threat to local populations, visitors, and animals (e.g., Chiodini et al., 2010; Granieri et al., 2013; Barberi et al., 2019, 2007; Viveiros et al., 2023, 2016). Such systems thus deserve special attention not only for monitoring volcano-tectonic processes (Boudoire et al., 2018), but also due to their potential direct impact on local populations and ecosystems (Pfanz et al., 2019; Vaselli et al., 2003).

At volcanic lakes, long quiescent periods favour the accumulation of

---

gases in the deepest water layers (Rouwet et al., 2014). Sudden exsolution of gas stored at depth and/or lake overturn can be triggered by both natural causes, such as earthquakes, landslide, gas saturation and water chemistry (Sigurdsson, 1988; Tazieff, 1989), or anthropogenic triggers, including climate change (Thuiller, 2007). The result is a limnic eruption and atmospheric dispersion of CO_2, where CO_2 enrichment of the air becomes a major health issue once the content exceeds 5 vol% (%), where the atmospheric background is around 0.042% CO_2 (420 ppm; https://www.cdc.gov/niosh/docs/76-194/). Investigation of limnic eruptions began in 1986, when >1700 people down-valley of Cameroon's lake Nyos (Kling et al., 1987; Sigurdsson et al., 1987; Boehrer et al., 2021) died by asphyxia following the sudden release of CO_2 (30×10^6 m^3, Freeth, 1990; 6×10^8 m^3, Faivre Pierret et al., 1992). Carbon dioxide (CO_2) is a colourless, odourless, and denser-than-air gas species, having a density of 1.87 kg m^{-3} (at 15 °C and 1013 hPa compared to 1.23 kg m^{-3} for air Lide, 2003). The density of CO_2 favours ground-hugging flow, so that it can spread at ground-level for several kilometres during a limnic eruption, where excess CO_2 in the air was recorded up to 20 km from the emission source at lake Nyos (Costa and Chiodini, 2015; Faivre Pierret et al., 1992; Folch et al., 2017). Thus, since 1986 interest in "Nyos-type" lakes has grown steadily (Barberi et al., 1989; Baxter et al., 1989; Camus et al., 1993; Faivre Pierret et al., 1992; Giggenbach et al., 1991; Kling et al., 1987; Tazieff, 1989), especially in long-dormant volcanic provinces where risk mitigation is poorly constrained.

In Europe, many long-dormant volcanic provinces host lakes marked by gas emissions. Lake Albano, around 20 km south-east of Rome, Italy (Anzidei et al., 2008; Cabassi et al., 2013; Carapezza et al., 2008; Funiciello et al., 2003; Martini et al., 1994; Rouwet et al., 2019) contains CO_2 that is released each year due to thermal convection of the water (seasonal overturn) (Chiodini et al., 2012). Convection prevents the accumulation of CO_2 a depth, unlike at a permanently stratified lake (meromictic lake), such as lake Nyos. However, lake Albano is monitored for anomalous CO_2 recharge that may occur during seismic events

(Chiodini et al., 2012; Rouwet et al., 2020). The Laacher See, the largest lake in the Eifel region of Germany (surface area: 3.3 km^2), is a holomictic lake, with a complete seasonal inversion of its water column at least once a year. Consequently, no CO_2 is stored at depth for the Laacher See. Instead, the lake discharges a significant amount of CO_2 gas in the form of a gas bubble plume as identified using an echo sounder (Goepel et al., 2015; Jouve et al., 2021). Such a system is known as a "wet mofette".

In this study, we focus on lake Pavin ("lac Pavin" in French) in the French Massif Central (Fig. 1). Lake Pavin is the site of the most recent eruptive activity in mainland France, with the last eruption being about 7 ka ago (Boivin et al., 2011; Juvigné and Miallier, 2016). The lake Pavin is the only meromictic lake known in France (Olivier, 1952; Pelletier, 1963, 1968) and, although previous studies have shown that a limnic eruption seems unlikely (Camus et al., 1993; Jézéquel et al., 2011), CO_2 is currently stored at depth. We note, though, that local archives suggest active degassing historically, including "boiling" activity in the eighteenth century (Meybeck, 2016a, 2016b). It is thus essential to estimate the amount of CO_2 currently stored at depth, and to investigate potential scenarios of CO_2 dispersion in the air in case of eruption. Critically, the presence of inhabited areas around the lake, and the presence of a high number of tourists, makes for a high-risk scenario. We thus develop an approach that combines gas geochemistry and atmospheric gas dispersion modelling to assess the impact of a potential limnic eruption of lake Pavin.

2. Study site

The European Cenozoic Rift System, which extends from southern France to Bohemia, hosts many quiescent volcanic provinces, such as that of the French Massif Central which covers an area of about 85,000 km^2. The last known eruptive event in mainland France occurred at the Pavin maar, which was formed by a phreatomagmatic eruption about 7000 years ago (Glangeaud, 1916; Leyrit et al., 2016). The Pavin maar,
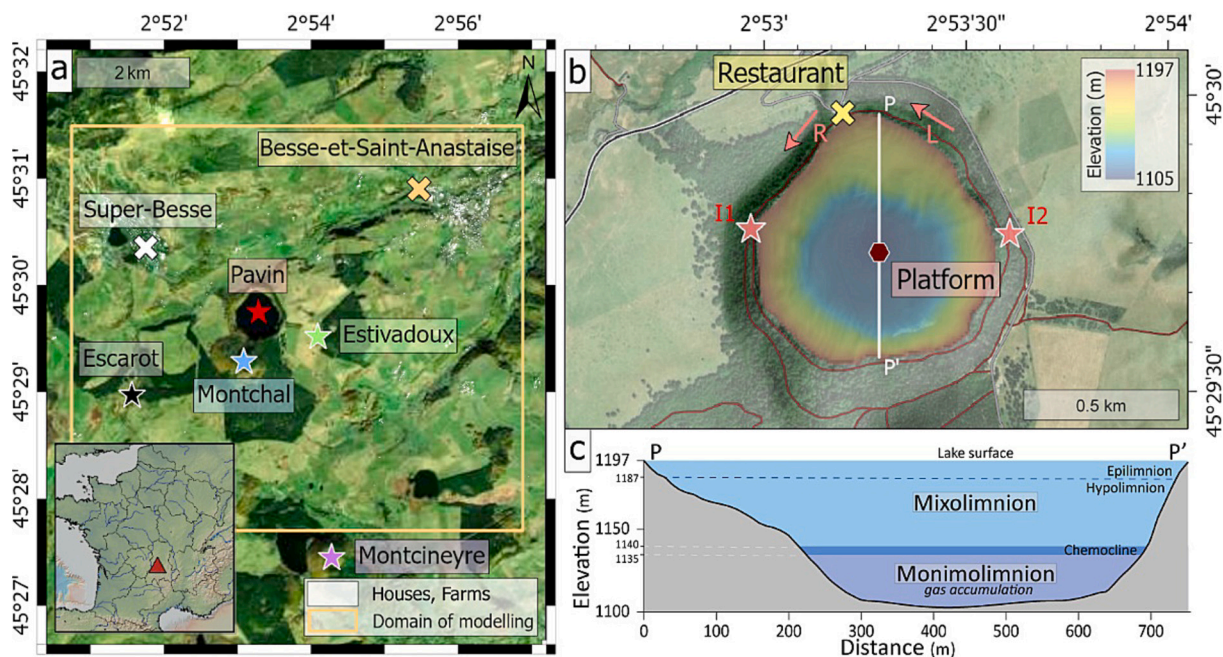
Fig. 1. (a) Location of the edifices of the Pavin's Group of Volcanoes (Montcineyre, Estivadoux, Montchal, lake Pavin) and of the dry CO_2 mofettes (Escarot). The location of the municipality of Besse-et-Saint-Anastaise and the Super-Besse ski resort are represented with an orange and a white cross respectively. The domain for the gas dispersion modelling is represented with an orange square. (b) Zoom on the lake Pavin with the location of the hiking trails (red lines). I1 and I2 are the intersections that allow exiting the main hiking path around the lake. The arrows R (right) and L (left) represent the established direction of circulation on the main hiking path starting from the yellow cross, which is the location of a restaurant (entry point). The burgundy point on the P-P′ line highlights the deepest point of the lake. (c) North-South bathymetric profile of the lake Pavin with the stratified layers. Service Credit Layers: Maxar Technologies, Microsoft: ESRI and Google Earth Pro; GeoMapApp and CRAIG. (For interpretation of the references to colour in this figure legend, the reader is referred to the web version of this article.)

together with three other volcanic constructs (Montcineyre, Estivadoux, and Montchal) make up the Pavin group of volcanoes (Fig. 1a) whose eruptive activity occurred over a period of just 100–700 years), with magma evolving from basanite to benmoreite during the period (Villemant et al., 2016). Although currently dormant, the area is still characterised by gas emissions through mineral springs and mofettes (Fig. 1a; Boudoire et al., 2023; Bräuer et al., 2017; Gal et al., 2018).

Located close to the municipality of Besse-et-Saint-Anastaise (4 km from the lake; Fig. 1a), Pavin maar (1197 m) is now filled by a sub-circular volcanic lake, about 750 m in diameter and with a surface area of 0.44 km^2 (Fig. 1b). Known to be the deepest lake in the region of Auvergne with a depth of 92 m and volume of 23.3×10^6 m^3; its U-shape favours the stratification of the water column making it a meromictic lake (Fig. 1c). This topography, marked by a great depth and a relatively small surface area, creates the phenomenon of stratification. The capacity of a lake to be stratified can be expressed by a dimensionless number, the "Depth Ratio", defined as the ratio between average depth to maximum depth (DR; Carpenter, 1983; Lehman, 1975), highlighting stratification for lakes with a value >0.45. At the lake Pavin, DR is 0.58, and thus greater than the limit of water stratification. With a DR higher than that of lake Nyos (DR = 0.55) or lago Albano (DR = 0.45) (Rouwet et al., 2019), lake Pavin is the only meromictic lake in France. The water column is divided into two distinct layers (Fig. 1c): (1) the mixolimnion, and (2) the monimolimnion separated by a chemocline at 60 m-depth (Aeschbach-Hertig et al., 2002, 1999; Camus et al., 1993). The mixolimnion (0–60 m-depth) is the upper layer of the lake and is well oxygenated and heated by the sun. This leads to a high level of biological activity at the surface (Assayag et al., 2008; Bonhomme et al., 2011). The mixolimnion layer is subject to wind effects and temperature variations that cause water circulation and mixing by convection (Dussart, 1966). This layer is itself divided into two layers. The first is the epilimnion, between 0 and 15 m. Below this is a thermocline that marks the transition to the hypolimnion that extends down to 60 m-depth (Delebecque, 1898; Pelletier, 1963). Below the chemocline (Fig. 1c), the monimolimnion is characterised by permanent anoxic conditions and an accumulation of dissolved gas, mainly CO_2 and CH_4 (Aeschbach-Hertig et al., 1999; Camus et al., 1993; Michard et al., 1994).

Many of lake Pavin's characteristics were defined as early as 1770, including lake depth (initially 96 m), bathymetry, water balance, water chemistry, and thermal anomaly at depth where the water is slightly warmer (Delebecque, 1898; Legrand d'Aussy, 1788; Meybeck, 2016a; Pelletier, 1963). Lake Pavin was first identified as a meromictic lake in the 1950's (Olivier, 1952; Pelletier, 1963, 1968), and was a target of increasing study after the lake Nyos event of 1986. The lake Nyos tragedy raised fears of possible sudden release of the gas accumulated in the monimolimnion layer at lake Pavin, so that vertical profiles for dissolved CO_2 were acquired (Aeschbach-Hertig et al., 1999; Camus et al., 1993; Michard et al., 1994; Olive and Boulègue, 2004). Results tended to rule out the risk of a sudden degassing episode, with a dissolved gas concentration in the monimolimnion being well below saturation and stable in time.

Although Camus et al. (1993) and Jézéquel et al. (2011) showed no risk of sudden degassing, past degassing events can be inferred from historic documents describing activity in 1551, 1783, and 1936 (Meybeck, 2016a, 2016b). In 1783, Godivel IV, chaplain of Besse, mentioned abnormal behaviour at lake Pavin, which he noted was renowned for its very clear water. Instead, on 21 August 1783 Godivel wrote that "the water is boiling everywhere but there is no wind, it is yellowish and even rusty in some places" (Meybeck, 2016b). Godivel assumed that this phenomenon, which he described as having occurred suddenly, was due to a landslide into the lake, which "disturbed large volume of water". The phenomena were again reported in 1936 (Joanny, 1987, 1986; Meybeck, 2016b) when a witness, Paul Joanny, described the lake as having a yellow-orange colour with a strong smell in the air. Similar observations were reported at lake Nyos some years later (Baxter et al., 1989; Kling et al., 1987).

In the past, approach to lake Pavin has been discouraged, mostly because of local superstition and the absence of a well-developed means of access (roads, footpaths, etc.). Only in 1859 was there the development of a path from the town of Besse to the lake following an initiative by Lecoq, a French naturalist. Then, in 1909 hiking trails were set up around the lake by the municipality of Besse-et-Saint-Anastaise (Meybeck, 2011; Fig. 1b). Today, lake Pavin is one of the most visited sites in the Auvergne region, with about 200,000 visitors per year (https://ens.puy-de-dome.fr/les-ens/lac-pavin-et-creux-de-soucy.html). Together with the 1500 inhabitants of the municipality of Besse-et-Saint-Anastaise, and a high flux of traffic on the road below the lake and up to the resort of Super-Besse during the ski season (Fig. 1a), lake Pavin could be considered at risk when gas-related hazard is facing with human exposure. This raises the question: what would happen if CO_2 currently dissolved in the monimolimnion layer were suddenly released?
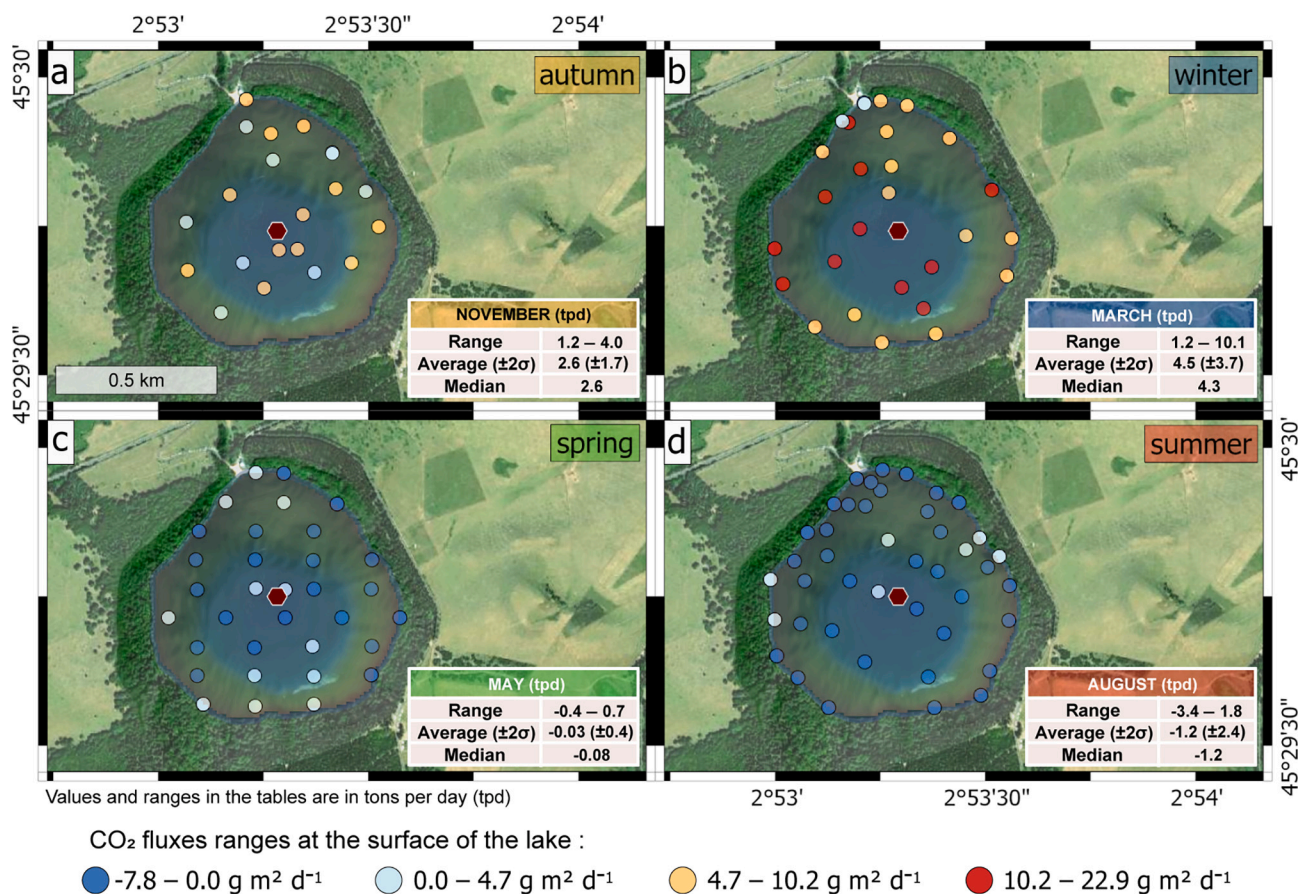
3. Methods

3.1. Field measurements

3.1.1. CO_2 flux at the surface of the lake

CO_2 flux measurements at the surface of lake Pavin were carried out using the accumulation chamber method (Andrade et al., 2021; Chiodini et al., 1998; Mazot et al., 2014, 2011; Viveiros et al., 2023). Measurements were made in November 2021, March 2022, May 2021, and August 2022, to characterise conditions in autumn, winter, spring, and summer, respectively. A total of 123 CO_2 flux measurements were performed distributed over the four seasons: 20 in autumn (Fig. 2a), 27 in winter (Fig. 2b), 33 in spring (Fig. 2c) and 43 in summer (Fig. 2d). A small fisherman's boat was used to carry out the measurements, making regular sampling challenging, especially given the unfavourable windy conditions in autumn and winter. For this reason, the positions of the measurement points were not regular. Consequently, minimum, maximum, and average flux values were used to discuss the current degassing of the lake over a surface of 0.44 km^2. Measurements in May (spring) 2021 were made with a temperature-stabilised LI-COR LI-820 infrared sensor (0–20,000 ppm CO_2), with a detection limit of 1.5 ppm and an accuracy of 3%. The sensor was connected to a West-Systems C-type accumulation chamber (diameter 300 mm, height 100 mm) with a floating ring allowing flux measurement over a water surface. Subsequent field campaigns (November 2021, March 2022, and August 2022) were carried out with the same West-Systems accumulation chamber, but with a portable CO_2 analyser EGM-5 (Environmental Gas Monitoring) from PP-Systems, with temperature and pressure compensation. The EGM-5 has a CO_2 range of up to 50,000 ppm (5%) and an accuracy of <1% over the calibrated range. For each measurement, CO_2 accumulating in the West-Systems chamber was recorded every second over a period of 120 s. Data were then processed with West-Systems Flux Revision software to obtain CO_2 flux (https://www.westsystems.com/instruments/download/). Calculation of CO_2 flux (g m^{-2} d^{-1}) is based on the regression of the accumulated CO_2 content (ppm s^{-1}) measured at the surface of the lake, the volume and surface area of the accumulation chamber, and the pressure and temperature of the ambient air (acquired with a Kestrel 5500 portable weather station).

3.1.2. CO_2 budget in the lake

During May 2021, two vertical profiles of both the physical (temperature, conductivity, and pressure) and chemical (pH and alkalinity) properties of the water were made at the site of the maximum depth (92 m; Fig. 1b). To guarantee a vertical profile, a weight was attached to the probes, and data acquisition was made at a 1 s interval during the descent and ascent of the probe system. Profiles were carried out at the same location as previous sampling (cf. Aeschbach-Hertig et al., 2002, 1999; Alvenerie et al., 1966; Camus et al., 1993; Delebecque, 1898; Lopes et al., 2011; Michard et al., 1994; Olive and Boulègue, 2004;

Fig. 2. Location of CO_2 flux measurements on the surface of the lake Pavin using the accumulation chamber method in (a) autumn, (b) winter, (c) spring, and (d) summer. The deepest point of the lake is represented by the burgundy polygon. The CO_2 flux is divided into four classes ranging from negative values in dark blue to positive values in red (see text for explanation). Service Credit Layers: Maxar Technologies, Microsoft: ESRI, Google Earth Pro and CRAIG. (For interpretation of the references to colour in this figure legend, the reader is referred to the web version of this article.)

Pelletier, 1968; Viollier, 1995; Zimmer et al., 2016). That is, they were made at a permanently anchored platform above the deepest point of the lake (Fig. 1). As we describe next, these were used to estimate the budget of dissolved CO_2 following methodologies reviewed in Boehrer et al. (2021) and Kusakabe et al. (2000).

3.1.2.1. Physical properties of the water: temperature and conductivity. Temperature, conductivity and pressure were measured using a VanEssen CTD-Diver probe (https://www.vanessen.com/products/data -loggers/ctd-diver/), where the pressure sensor that measures the equivalent hydrostatic pressure above the sensor diaphragm to determinate depth with a 5 cm-accuracy. The probe is also equipped with a conductivity sensor that measures electrical conductivity up to 120 mS cm^{-1} with an accuracy of 1%. A temperature sensor was included providing measurements with an accuracy of 0.1 °C.

3.1.2.2. Chemical properties of the water: pH and alkalinity. Water sampling for pH and alkalinity was performed using a pump connected to a 100 m-long PVC tube to which a stainless-steel funnel was attached. Samples were taken in (1) the mixolimnion layer (samples PAV3–1 and PAV6–1 at 0 and 30 m, respectively), (2) the monimolimnion layer

(samples PAV5–1 and PAV1–1 at 80 and 92 m, respectively), and (3) at the interface between the two layers (samples PAV4–1 and PAV2–1 at 58 and 61 m, respectively). A HI98195 HANNA portable probe and a HI3811 HANNA alkalinity test kit (0–300 mg L^{-1}) were used onsite to measure pH (accuracy: ±0.02) and the total alkalinity (TAC) of the water samples. Based on the previous chemical measurements performed by Michard et al. (1994) at lake Pavin, we assumed that the carbonate alkalinity was equal to the total alkalinity. Measurements of pH measurements were systematically lower than 8.3. This means that there was an absence of carbonate ions CO_3^{2-}, so that the $CaCO_3$ alkalinity is equivalent to the HCO_3^- content (i.e., 1 mg L^{-1} of $CaCO_3$ = 1.23 mg L^{-1} of HCO_3^-; https:// www.hannainst.com/hi3811-alkalinity-test-kit.html).

3.1.2.3. Estimation of the amount of dissolved CO_2. To estimate the amount of CO_2 dissolved the lake, we used the indirect approach of Kusakabe et al. (2000). This is based on the linear relation between water conductivity and HCO_3^- content, which is equivalent to the total alkalinity because pH was <8.3. The HCO_3^- content across the water column was thus estimated from the conductivity vertical profile (CTD probe) through the linear relationship established with the six water samples:

$$\text{Alkalinity or } HCO_3^- \left(\text{mol L}^{-1}\right) = (0.000011 \times \text{conductivity}(25°C; \mu S \text{ cm}^{-1})) + 0.000053;$$
$$R^2 = 0.96$$

(1)

Salinity was then obtained from the relationship between conductivity and temperature given by Aminot and Kérouel (2004). By combining the HCO_3^- content, salinity, pH, and temperature, the total amount of dissolved carbon $(HCO_3^- + H_2CO_3 + CO_3^{2-})$ and its speciation in water at equilibrium was retrieved following Millero and Pierrot (1998). This was done of for each 5 m-thick water layers down the water column. To estimate the total amount of dissolved CO_2 in the lake, the volume of each 5 m-thick layer from the surface to the bottom of the lake was calculated. To do this, we used the bathymetric data provided by BRGM (Bureau de Recherches Géologiques et Minières[3]) and obtained on 10 June 2008 using multibeam acoustic sounding with a 240 kHz sounder. Using the 3D analysis toolbox of ArcMap (ArcGIS) (https://desktop.arcgis.com/en/arcmap/latest/tools/3d-analyst-toolbox/), we estimated the water volume present below a reference altitude of 1197 m, as well as volume of water in each 5-m and 10-m of layer.

3.1.2.4. Composition of the gases dissolved in the monimolimnion layer. Dissolved gases in the monimolimnion reached saturation in water at atmospheric pressure and thus exsolved during sampling. Gas was sampled at 80 m-depth by using a 100 m-long PVC tube (graduated each meter) immersed vertically (with a load attached to the end). Water was pumped through the tube and the gas phase exsolved during the water ascent was trapped in glass samplers connected to a three-way glass tap. Successive analyses (*for $CH_4, CO_2, N_2, O_2, CO, He$ and H_2*) were performed at the Istituto Nazionale di Geofisica e Vulcanologia – Sezione di Palermo using a gas chromatograph (GC, Agilent 7890 equipped with PPU and MS5A column), a MicroGC module (equipped with a PPU column), and a double detector (TCD and FID) with argon as the carrier gas. Analytical errors were <3%.

3.2. Numerical modelling

Atmospheric gas dispersion can be passive (i.e., dominated by advection-diffusion through the atmospheric wind field, turbulence, and gas concentration gradient) or density-driven (i.e., governed by positive buoyancy for hot gases and negative buoyancy for cold gases). To characterise the gas dispersion regime, we use the Richardson number, R_i (Britter and McQuaid, 1988; Cortis and Oldenburg, 2009):

$$R_i = \frac{1}{v^2}\left(\frac{g' q}{R}\right)^{\frac{2}{3}} \tag{2a}$$

where q is the volumetric flow rate ($m^3 \ s^{-1}$), R is the characteristic length of the plume (m), and v is wind speed ($m \ s^{-1}$) at the reference altitude. Reduced acceleration due to gravity (g') is given by:

$$g' = g(\rho_g - \rho_a)/\rho_a, \tag{2b}$$

in which g is acceleration due to gravity ($m \ s^{-2}$), and ρ_g and ρ_a are the density of the gas and air, respectively ($kg \ m^{-3}$). Following Cortis and Oldenburg (2009), the Richardson number allows us to determine whether dispersion is passive, ($R_i < 0.25$), or density-driven ($R_i > 1$). The interval $0.25 < R_i < 1$ separates the two turbulent regimes, associated with strong and weak mixing, respectively (Costa et al., 2005; Costa et al., 2013; Costa and Macedonio, 2016).

Two open-source codes were used to model gas dispersion. The first, DISGAS v. 2.1 (Costa and Macedonio, 2016; http://datasim.ov.ingv.it/models/disgas.html), is valid for passive dispersion conditions (i.e., a dilute plume). The second is TWODEE-2 v. 2.6 (Folch et al., 2009; Hankin and Britter, 1999a, 1999b, 1999c; http://datasim.ov.ingv.it/models/twodee.html) was used to model flows that follow the topography under gravity-driven conditions. Both DISGAS and TWODEE-2

outputs gas concentration at different heights above the ground providing gas concentrations that exceed the background air concentration, which for CO_2 is ca. 420 ppm. A Diagnostic Wind Model (DIAGNO; Douglas and Kessler, 1990) is coupled to these two codes in order to model zero-divergence wind fields over a complex topography. The zero-divergence in DIAGNO domain implies the conservation of mass within a region (in this case, our domain). It means that the air is neither accumulation nor depleting within that region, which is a fundamental principle used in atmospheric modelling.

The probabilistic maps were created using VIGIL v. 1.3.5 (Dioguardi et al., 2022, https://github.com/BritishGeologicalSurvey/VIGIL), an automatic workflow composed of three Python scripts. These allow (1) recovery and processing of the meteorological data, followed by (2) launch DIAGNO, and DISGAS or TWODEE-2 depending on the Richardson number, and (3) statistical analysis of the output to provide graphic representations of simulations, i.e., probabilistic hazard maps. For the probabilistic hazard map, the user needs an interval of confidence, set at 95% in this study. We used a total of 315 days of meteorological data obtained by two stations (Super-Besse, Fig. 1; and Clermont-Ferrand, 50 km north-east of the lake) operated by the Laboratoire de Météorologie Physique (LaMP, Aubière, France) and provided by Météo-France (available at http://publitheque.meteo.fr/okapi/accueil/okapiWebPubli/index.jsp). The dataset covers all four seasons (16 days of data per season) for five years between 2016 and 2020. This allows us to obtain a representative trend of the meteorological conditions for each season. We chose local Météo-France stations instead of e. g., the ERA-5 reanalysis data provided by the ECMWF (Hersbach et al., 2020) which are given with a coarser horizontal resolution than the local Météo-France stations. A comparison between the ERA-5 (over the 1981–2010 period) and the Météo-France (over the selected period) data for the temperature, wind speed and direction validates the representativeness of the Météo-France meteorological trends used in this study; Météo-France data are quite similar than the ERA-5 data for the minimum, maximum and mean values (Supplementary material: Fig. S1, S2). The station located at Clermont-Ferrand airport (45°47′13″N, 3°08′58″E), provides temperature and atmospheric pressure at an altitude of 331 m, this being the Météo-France station with a pressure measurement closest to the lake. The second station is located <2 km from lake Pavin at Super-Besse (45°30′06″N, 2°51′57″E; Fig. 1), and provides temperature and wind speed data at an altitude of 1287 m. Assuming an adiabatic lapse rate of 6.5 °C per 1000 m of elevation gain (Roe and O'Neal, 2009; Wallace and Hobbs, 2006), there is a negligible temperature difference of -0.59 °C between Super-Besse and lake Pavin. The wind data are assumed to be similar at the Super-Besse station and at the lake Pavin. However, it is important to keep in mind that in the mountains areas valleys can locally intensify the flow (Planche et al., 2013), so that the wind speed down the valley between Super-Besse and at lake Pavin may have been higher. As the pressure (in hPa) was not available at the altitude of the lake ($P_{superbesse}$), we applied a correction to the atmospheric pressure measured at the airport in Clermont-Ferrand ($P_{airport}$) using the hypsometric equation of Colella (2005) and a standard atmosphere:

$$P_{Superbesse} = P_{airport} * \left(\frac{T_{superbesse}}{T_{airport}}\right)^{-\left(\frac{g}{\left(\frac{\Delta T}{\Delta z}\right)*R}\right)} \tag{3a}$$

where $T_{superbesse}$ and $T_{airport}$ the temperatures for the two stations (K), $\Delta T/\Delta z$ is the temperature gradient ($K \ m^{-1}$), and R is the specific gas constant for dry air ($J \ kg^{-1} \ K^{-1}$) as calculated from:

$$R = R'/M_a \tag{3b}$$

here, R' is the universal gas constant ($J \ K^{-1} \ mol^{-1}$) and M_a is the molar mass of dry air ($kg \ mol^{-1}$).

---

[3] Made through a contract with the MESURIS company at the request of the Direction Départementale de l'Equipement du Puy-de-Dôme.

Numerical modelling also requires a Digital Elevation Model (DEM), which was obtained from the Auvergne-Rhône-Alpes regional centre for geographic information (www.craig.fr). The cell size used for both DISGAS and TWODEE-2 was 30 m and 25 m, respectively. Given a region of interest (ROI) of 7.8 × 6.9 km, this involved a DEM of 260 × 230 cells for DISGAS, and 312 × 276 cells for TWODEE-2.

3.3. Risk assessment

To assess the risk posed by a flow of CO_2 released by a limnic eruption at lake Pavin we collected data for the number of tourists visiting the lake in each season and identified the location of the main hamlets and villages with each ROI. For the latter, we identified all houses in the study area (within a radius of around 5 km the lake) using

Google Earth. For visitor counts we chose a day during the school holidays or a weekend, to be close to the upper limit for the number of agents onsite in each season and made counts in each of the four seasons. Three categories of individuals were distinguished: (1) visitors who went no further than the entrance of the lake (Fig. 1b) where the main, roadside, viewpoint, and bar/restaurant, (2) hikers who completed the hike around the lake, and (3) hikers leaving (or arriving on) the path network that extends to the south or south-east of the lake, and thus completing only a partial tour of the lake before accessing the trail network (Fig. 1b). This last category was based on the difference between the number of people starting the tour and those returning to the entrance point.
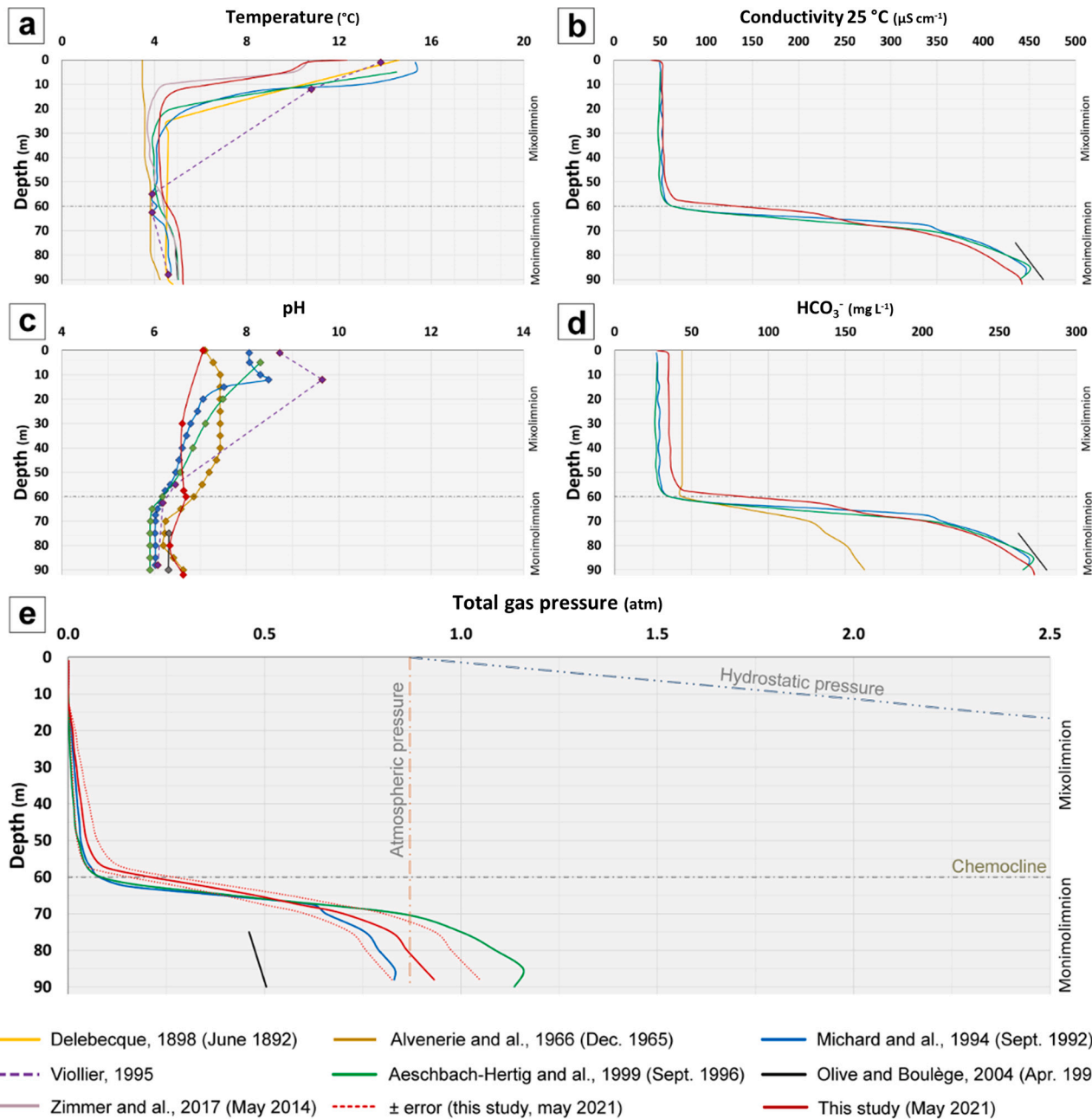

Fig. 3. Profile of (a) temperature, (b) conductivity, (c) pH, (d) alkalinity, and (e) estimation of the total gas pressure in the lake Pavin. The results of this study are highlighted by the red line. The dashed lines represent the uncertainty by considering the error propagation on pH, temperature, alkalinity, and salinity measurements. The results of previous measurements (with dates in parentheses) are shown for comparison. (For interpretation of the references to colour in this figure legend, the reader is referred to the web version of this article.)

4. Results

4.1. CO₂ flux at the lake surface

Using the maximum-likelihood method of the SoilExp software (Boudoire et al., 2020), four populations of CO_2 flux were found (Fig. 2). Three populations include positive fluxes between 0.0 and 22.9 g m^{-2} d^{-1}, and one includes negative fluxes between −7.8 and 0.0 g m^{-2} d^{-1}. The population marked by highest CO_2 fluxes occurs during the winter, just after the ice sheet covering the lake has melted. The population marked by negative CO_2 fluxes occurs during the summer. This cycle is well known for meromictic lakes under temperate climatic conditions and is related to two phenomena: (1) lake overturn in late autumn and late winter (Bonhomme et al., 2016; Jézéquel et al., 2016), and (2) photosynthesis during summer (Dussart, 1966; Jézéquel et al., 2016). The first phenomenon results from water circulation when the surface water becomes denser (triggered by cooling) than the water upon which it lies. The second phenomenon is a biological process that allows microorganisms, algae, submerged plants, and floating plants to absorb the sunlight that penetrates the water, using chlorophyll pigments in their cells. In this way the lake absorbs CO_2.

Our CO_2 flux estimates across the whole surface of the lake give 2.6 ± 1.7 tons/day in autumn and 4.5 ± 3.7 tons/day in winter. Instead, a CO_2 flux of 0.0 ± 0.4 tons/day is observed during the spring, and a negative flux of −1.2 ± 2.4 tons/day in the winter. In comparison, in June 2010, Jézéquel et al. (2011) obtained an average CO_2 flux of 0.3 ± 0.03 tons/day. These values were obtained at the end of spring 2010 and lie in the range of those that we measured in May 2021 (0.0 ± 0.4 tons/day).

4.2. Gas budget in the monimolimnion layer

The temperature profile measured in May 2021 is similar to those obtained since 1898 (Fig. 3a). Between the surface and 15 m (the epilimnion layer), temperature gradually decreases from 12.3 °C to 4.6 °C. Our temperatures are slightly lower than previously recorded (Fig. 3a), but it is worth noting that other field campaigns were performed between May and September, when higher air temperatures may lead to temperature variations in the epilimnion layer (Aeschbach-Hertig et al., 1999; Alvenerie et al., 1966; Delebecque, 1898; Michard et al., 1994; Olivier, 1952; Pelletier, 1968; Viollier, 1995; Zimmer et al., 2016). The temperature of the underlying water column is almost constant with temperature ranging from 4.3 to 5 °C, as in all previous measurements.

The May 2021 conductivity profile varies from 40.4 to 442.1 μS cm^{-1} between 0 and 92 m, and that is similar to the range of 49.6 to 445.5 μS cm^{-1} obtained in 1992 by Michard et al. (1994). A sudden inflexion in conductivity occurs at 60 m (Fig. 3b) and marks the chemocline, i.e., the transition from the mixolimnion (0–60 m; 40.4–69.8 μS cm^{-1}) and the monimolimnion (60–92 m; 134.2 to 442.1 μS cm^{-1}). The depth of the chemocline is same as that recorded in previous studies (Fig. 3b).

The pH was profile differs from previous profiles (Fig. 3c). As measurements were not made in-situ (but a few hours after sampling), we suspect that post-sampling processes (precipitation, degassing) modified the original signature. For this reason, and considering the good agreement of our conductivity and temperature measurements with previous studies, we instead use the pH profile of Michard et al. (1994). In this profile (the one with the highest resolution along the whole water column in literature), pH continuously decreases with depth from 8 at the surface to around 6 at the lake floor.

Alkalinity was calculated from the conductivity using eq. (1) and does not differ from previous measurements (Fig. 3c). The profile is marked by an inflexion at the chemocline, with a shift from 28 to 46 mg L^{-1} in the mixolimnion to 272 mg L^{-1} in the monimolimnion. This compares with maximum from previous measurements of 163 mg L^{-1}, 269 mg L^{-1}, 272 mg L^{-1}, and 281 mg L^{-1} (Alvenerie et al., 1966;

Michard et al., 1994; Aeschbach-Hertig et al., 1999; Olive and Boulègue, 2004). In general, our measurements confirm stability of the physico-chemical parameters of the lake on a temporal scale of decades.

We estimated the total volume of water in the lake as being approximately 23.3 × 10⁶ m³ (± 6%). The mixolimnion hosts 19 × 10⁶ m³ (82%) of the lake water, whereas the remaining 4.3 × 10⁶ m³ is accounted for by the monimolimnion. Using pH measurements of Michard et al. (1994), we retrieve the amount of dissolved carbon and its speciation as a function of depth for each 5 m-thick water layers. Considering current pH profile of the lake (from 8 to 6), this gives a value for dissolved CO_2 (cf. H_2CO_3) in the monimolimnion of 1748 ± 279 tons (~1750 tons), which overlaps the 1800 tons estimated in 2010 by Jézéquel et al. (2011). In the case of a full conversion of the current HCO_3^- into H_2CO_3 (theorical decrease in pH from 6 to 4) the dissolved CO_2 in the monimolimnion would be 2338 ± 337 tons (~2350 tons). This last case and its interest will be discussed later.

To simulate potential scenarios of limnic eruption involving the monimolimnion layer, the amount of CO_2 available for exsolution at atmospheric pressure (in the event of water ascending to the surface) was estimated. To do this we used Henry's constant (for the CO_2 partial pressure – P_{CO2}; Wilhelm et al., 1977; Mackay et al., 2000), the measured gas composition (with CO_2, CH_4, and N_2 accounting for 99.99% of the gas composition; Table 1), and the partial pressure of the gases (P_{CO2} for carbon dioxide, P_{CH4} for methane, and P_{N2} for nitrogen) from:

$$P_{CO_2} = \frac{[H_2CO_3]}{K_H}; P_{CH_4} = 2.97 \times P_{CO_2};$$
$$P_{N_2} = 0.41 \times P_{CO_2} \tag{4}$$

here $[H_2CO_3]$ is the concentration of dissolved CO_2 in the lake, and K_H Henry's constant. The constants, 2.97 and 0.41, correspond to the CH_4/CO_2 and N_2/CO_2 ratios measured here (Table 1). The CH_4/CO_2 measured by us is in the range of previous measurements (1.66–22; Camus et al., 1993). To calculate the total gas pressure for each 5 m-thick layers (Fig. 3e), we assumed a constant gas composition (and thus constant gas ratio) for the entire monimolimnion layer. Resulting total gas pressure ($P_{TOT} = P_{CH4} + P_{CO2} + P_{N2}$) displays a change at the chemocline. Considering 1750 tons of dissolved CO_2 in the monimolimnion (current state), P_{TOT} does not exceed, hydrostatic pressure but is above atmospheric pressure ($P_{atm} = 0.87$ atm at the surface of lake Pavin) between 80 and 92 m. The effect of this was observed by the presence of gas bubbles, in water samples collected at 80 and 92 m depth, when the water reached the surface. We consequently estimate the quantity of dissolved CO_2 between 80 and 92 m that is available for a release in the atmosphere (i.e., satisfying $P_{TOT} = P_{atm}$ at the end of the limnic eruption) if the waters of the monimolimnion layer reach the surface. Our calculations highlight that 445 tons (~450 tons) of dissolved CO_2 (over the 1750 tons of total dissolved CO_2) are currently available for a release into the atmosphere. In the case of a full conversion of the current HCO_3^- into H_2CO_3 (theorical decrease in pH from 6 to 4), P_{TOT} would remain below the hydrostatic pressure but would exceed P_{atm} between 70 and 92 m. In this case, we estimate a quantity of dissolved CO_2 of 1772 tons (~1750 tons) available for a release into the atmosphere (over the 2350 tons of total dissolved CO_2).

4.3. Weather conditions

To model atmospheric CO_2 dispersion, wind speed data and gas source conditions are needed to assess whether the gas will be transported buoyantly in the atmosphere, or whether it will flow along the ground. A two-week period of hourly measurements was considered for each season during the five years spanning 2016–2020 in autumn, winter, spring, and summer (Fig. 4). Four wind speed-dependent classes (0–4 m s^{-1}, 4–8 m s^{-1}, 8–12 m s^{-1} and >12 m s^{-1}) were identified. The prevailing wind direction is from the northwest to the southwest (Fig. 4).

Table 1

Gas composition of sample LP 5–1 (raw and corrected data), collected at 80 m-depth at the platform.

Site								
Area	Source	Type	Town	Latitude (N)	Longitude (E)	Label	Date	
Monts-Dore	lake Pavin	Lake	Besse-et-Saint-Anastaise	45°29′45″	2°53′17″	LP 5–1	26/05/2021	

Raw composition (μmol/mol)									
CO_2	O_2	N_2	Ar	He	H_2	CO	CH_4	Total	X_{air}
219,500	3900	105,600	–	14	4	44	652,100	981,162	0.019

Corrected composition (μmol/mol)									Ratio
CO_2	O_2	N_2	Ar	He	H_2	CO	CH_4	Total	CH_4/CO_2
223,657	0	92,790	–	14	4	45	664,471	980,981	2.97

Corrected value are the raw data corrected for air contamination (X_{air}: fraction of air in the gas sample; see Methods). In red, the CH_4/CO_2 ratio like previous measurements made at the lake Pavin.
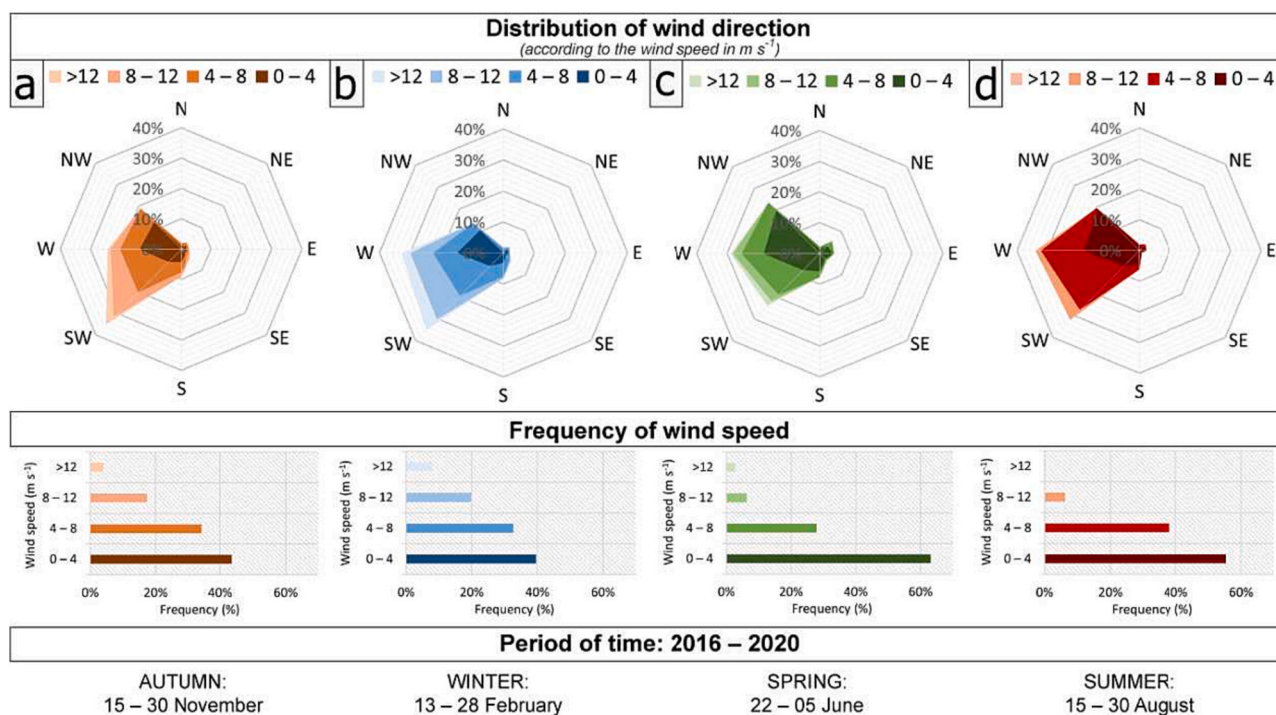
Fig. 4. Wind directions, velocity, and frequency as a function of the wind speed (divided in 4 classes) considering two-week period of hourly measurements for each season during five years (2016–2020): (a) 16 × 5 days in autumn, (b) 16 × 5 days in winter, (c) 15 × 5 days in spring, and (d) 16 × 5 days in summer.

Table 2

Statistics of intensive weather parameters by season for a period of five years (2016–2020).

		AUTUMN	WINTER	SPRING	SUMMER
Wind speed (m s^{-1})	*Min*	0.0	0.0	0.0	0.0
	Max	19.0	20.1	14.3	13.1
	Average	5.0	5.7	3.8	3.8
	Median	4.3	5.0	3.3	3.5
Temperature (°C)	*Min*	−6.7	−17.0	1.0	5.0
	Max	16.1	18.6	23.6	29.4
	Average	3.1	1.7	11.9	16.2
	Median	3.3	2.2	11.7	16.0
Pressure (hPa)	*Min*	845.8	844.2	858.1	863.3
	Max	885.2	886.2	886.5	885.2
	Average	869.2	872.1	873.6	875.9
	Median	869.3	873.6	873.4	876.3

Temperature and wind speed are taken from the Météo-France station at Super-Besse (altitude: 1287 m). The pressure corresponds to the calculated pressure at the altitude of the Super-Besse station using the Clermont-Ferrand airport Météo-France station (altitude: 331 m; see Methods).

In autumn (Fig. 4a), the weakest winds (<4 m s^{-1}) are predominantly from the west, whereas the strongest (>12 m s^{-1}) are from the south-west. Similar behaviour is observed in winter (Fig. 4b). This trend differs in spring (Fig. 4c) and summer (Fig. 4d), when the weakest winds (<4 m s^{-1}) are mainly from the northwest, while the strongest winds (>12 m s^{-1}) are from the west. Wind speed is mostly <4 m s^{-1}, which accounts for 44, 40, 63, and 55% of the records in autumn, winter, spring, and summer, respectively (Fig. 4; Table 2). Winds with highest speeds (>12 m s^{-1}) are the rarest, accounting for 4, 8, 3, and 0.3% of the records in autumn, winter, spring, and summer, respectively. Winter is the windiest season with an average speed of 5.7 m s^{-1}. Spring and summer have the lowest wind speeds, with averages of 3.8 m s^{-1}.

Average air temperature is +3.1, +1.7, +11.9, and + 16.2 °C in autumn, winter, spring, and summer, respectively. These air temperatures are either higher or lower than the lake water temperature (Fig. 3) according to the season, and favours lake overturn due to thermal convection (Boehrer et al., 2017). This biannual phenomenon explains the increase in CO_2 flux at the lake surface in late autumn and late winter (Fig. 2) through periodic ascent of CO_2-richer water from the

mixolimnion towards the surface. Atmospheric pressure is lower in autumn (869.2 hPa, on average) than for the other seasons (Table 2). The maximum atmospheric pressure is reached during the summer (875.9 hPa, on average).

4.4. Tourism and inhabited areas

A total of 2582 people were counted at the lake Pavin during our one-day surveys performed in each of the four seasons (Table 3). Lower numbers of visitors were recorded in the autumn (34/2582) and winter (153/2582), with respect to spring (467/2582) and summer (1928/2582). More than three quarters of the visitors on the four survey days used the hiking paths around the lake to make a total or partial tour, whatever the season: 1748 in summer (91%), 29 in autumn (85%), 146 in winter (95%), and 448 in spring (96%). Hiking was mostly anti-clockwise (from the west side towards the east side) following directional signs on the path; a route that takes about one hour to complete. It is possible to leave the main path to extend the hike and visit the other volcanoes of the complex (Montchal, Estivadoux and Montcineyre, Fig. 1). Over the whole year, 80% of visitors completed a total tour, 12% a partial tour, and 8% remained at the main entrance point where there is a restaurant and viewpoint (Fig. 1).

Apart from the two main settlements (population over 100), the village of Besse-et-Saint-Anastaise and the ski resort of Super-Besse, numerous hamlets (<100 inhabitants) are scattered around lake Pavin (Fig. 5c). Most are located immediately to the north, and below the outlet from lake Pavin, in the area of the "Plaine du Gelat", the Couze-Pavin valley and Sagnes (Fig. 5c). Other hamlets are located south-east of the lake in the Anglard-Vaucoux valley (Av) (Fig. 5c).

5. Discussion

5.1. Decision tree and choice of model for CO_2 dispersion

The total surface CO_2 fluxes estimated for lake Pavin, the dissolved CO_2 budget in the monimolimnion layer, and weather conditions are used as starting conditions to model potential atmospheric dispersion of CO_2 in the case of a limnic eruption. We consider three main scenarios: (*Scenario 1*) the current level of CO_2 degassing at the lake, (*Scenario 2*) a potential release of CO_2 currently dissolved in the monimolimnion layer, 450 tons of which would then exsolve at atmospheric pressure (see Results), and (*Scenario 3*) the potential release of the CO_2 accumulating in the monimolimnion layer if all current bicarbonates are converted to dissolved CO_2, i.e., releasing 1750 tons of CO_2. We use "CO_2 cloud" to
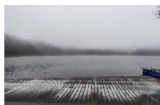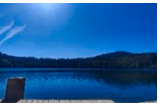
indicate the geographical area where CO_2 content in the air exceeds 5000 ppm (this being the 8 h-exposure maximum recommended by OSHA – the Occupational Safety and Health Administration). Our concentration maps show the CO_2 content in the air at a height of 1.50 m, as this represents an average inhalation height for a human being. Note that the quantity of CH_4 released in the case of limnic eruption would be the highest one but CO_2 is the only gaseous species of interest in this study for its density larger than the air that raises issues regarding gas dispersion at the soil-air interface.

In *Scenario 1*, the Richardson number remains low (0.009–0.014) whatever the season (Fig. 5a). The values of the Richardson number are <<0.25 and support the use of DISGAS (a wind-dominated model) to model CO_2 dispersion (e.g., Granieri et al., 2014; Massaro et al., 2022, 2021; Viveiros et al., 2023). In total, four runs were made for this scenario, one for each season. *Scenario 2* (Fig. 5b-i) is based on our estimation of current dissolved CO_2 in the monimolimnion that may be released if the deep water ascends to the surface. Landslides from the maar inner-flanks, earthquakes, changes in the physico-chemical conditions of the lake, and/or changes in thermal convection induced by climate change could be potential triggers of a limnic eruption at lake Pavin (Chapron et al., 2010; Thouret et al., 2021). *Scenario 3* (Fig. 5b-i) is an extreme scenario in which all the current bicarbonates would be converted in dissolved CO_2. It requires a drastic decrease of the pH (down to 4) that may be enhanced by the arrival of acidic fluids at the bottom of the lake where water emergences were reported (Boyd, 2000; Doney et al., 2009; Talling, 2010). These last two scenarios were run with the TWODEE-2 code since the associated Richardson numbers ranged from 0.20 to 0.68 (i.e., generally >0.25).

The sudden conversion of all the bicarbonates in dissolved CO_2 that would accumulates in the monimolimnion layer (*Scenario 3*) may appear unrealistic considering that the arrival of acidic fluids may generate other changes in the physico-chemical parameters of the lake as a convective movement of the waters favouring progressive CO_2 degassing (Caudron et al., 2017). On another side, the dynamics of CO_2 exsolution during limnic eruption are poorly constrained. In particular, it remains unclear if (1) the quantity of dissolved CO_2 released during a limnic eruption has to satisfy the relation P_{TOT} (total gas pressure dissolved in the water) = P_{atm} (atmospheric pressure) at the end of the eruption or if (2) the sudden gas exsolution may favour $P_{TOT} < P_{atm}$. In the latter case, for the *Scenario 2*, we calculated a quantity of dissolved CO_2 of 1750 tons available for a release into the atmosphere and satisfying $P_{TOT} = 0$ atm at the end of the limnic eruption (against 450 tons of total dissolved CO_2 if $P_{TOT} = P_{atm}$ at the end of the eruption). Casually, this quantity is similar to the one calculated for the *Scenario 3*. For this

Table 3

Count of individuals (adults + children) on a representative of high visitation day (during school holidays or weekends) for each season.

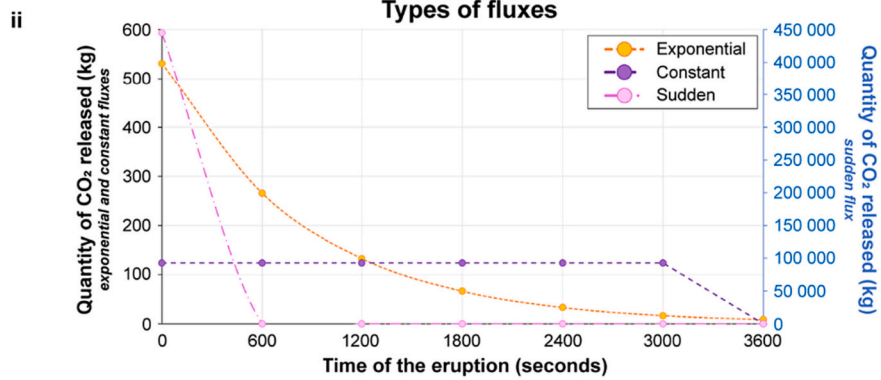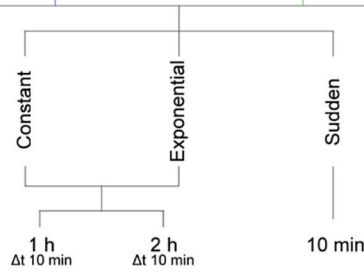|	AUTUMN	WINTER	SPRING	SUMMER
	Wed. 30th Nov. 2022	*Wed. 23rd Feb. 2022*	*Sun. 28th Mar. 2021**	*Wed. 24th Aug. 2022*
Total of people at the lake	**34**	**153**	**467**	**1928**
At the restaurant	5	7	19	180
On the hiking path	29	146	448	1748
Complete tour of the lake	*23*	*113*	*417*	*1509*
Partial tour of the lake	*6*	*33*	*31*	*239*
Weather	Snow, fog, and negative temperature	Snow, fog, and negative temperature	Sun and temperature above 20 °C	Sun and temperature above 25 °C

The total counting is divided into two categories: the number of people who stop at the restaurant (main entrance point to the lake) or the number of people who used the path around the lake. For the second category, we distinguished (1) people who complete the tour of the lake and (2) people who exit the main hiking path to access secondary hiking paths such as the one to Montchal (see Fig. 1). *Counting made during the third partial lockdown in France.

a Scenario **1** - DisGAS modeling　RN: Richardson number

Autumn	Winter	Spring	Summer
RN: 0.010	RN: 0.009	RN: 0.014	RN: 0.012

b Scenario **2 & 3** - TWODEE modeling

Quantity of CO_2 released
Scenario (2): **450 tons** (between 80 − 92 m of depth)
Scenario (3): **1,750 tons** (between 70 − 92 m of depth)

i

Autumn	Winter	Spring	Summer
(2) RN : 0.22	(2) RN : 0.20	(2) RN : 0.27	(2) RN : 0.23
(3) RN : 0.49	(3) RN : 0.54	(3) RN : 0.68	(3) RN : 0.57

Constant　　Exponential　　Sudden

1 h Δt 10 min　　2 h Δt 10 min　　10 min

ii

Tracking points (WGS84):
TP1 - 45°29.9636' N, 2°53.1985' E (restaurant of the lake)
TP2 - 45°30.9074' N, 2°55.4133' E (first houses of the city)

Levels of modeling:
0.20 cm — animals height
1.00 m ⎤ humans height
1.50 m ⎦ (children & adults)

c Digital Elevation Model and area
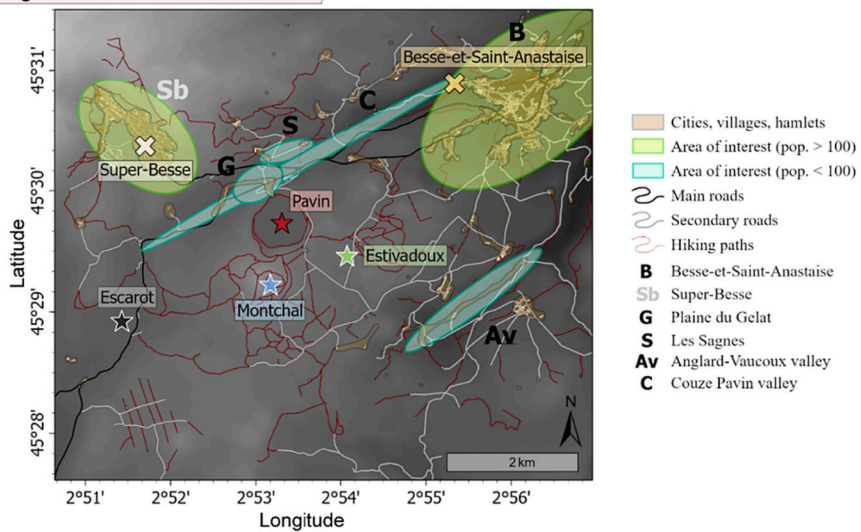
(caption on next page)

Fig. 5. Tree structure of the atmospheric CO_2 dispersion modelling performed in this study. (a) *Scenario 1* – Model (DISGAS) considering the current degassing measured at the surface of the lake for each season. (b) i – *Scenario 2 & 3* – Models (TWODEE-2) where the current and upper limit of dissolved CO_2 budget in the monimolimnion layer is released. ii – Graphical representation of the three different types of gas release used for modelling. The time evolution of the CO_2 content in the air was also continuously modelled at two tracking points: at the restaurant of the lake Pavin (main entrance) and at the first inhabited house of the municipality of Besse-et-Saint-Anastaise (in the Couze-Pavin valley). (c) Domain of modelling using the DEM of the lake Pavin (Puy-de-Dôme area). The domain allowed to distinguish all the different areas, in particular the populated areas as well as the roads, and hiking paths.

reason, *Scenario 3* is admittedly an extreme scenario, but it allows us to cover the uncertainty of *Scenario 2*, which is fundamental for risk assessment purposes.

In total, 40 models were run (20 for each scenario) covering each season (Fig. 5b), with two durations of limnic eruption and three types of gas release. The duration of limnic eruption represents the time required for total release of the dissolved CO_2. Durations of one and two hours were considered. Two hours of limnic eruption are an upper limit that allows comparison with other limnic eruption models, notably those for lake Nyos where durations of two and four hours were used (Costa and Chiodini, 2015; Folch et al., 2017). The choice of one hour highlights quicker release of CO_2 at lake Pavin as supported by the idea that available dissolved CO_2 is lower than the ones modelled at other meromictic lakes, such as Monoun and Nyos in the Cameroon (Costa and Chiodini, 2015; Kozono et al., 2017) and Kivu in the Democratic

Republic of Congo (Vaselli et al., 2015). The mechanism of gas release was modelled as (1) constant, (2) following an exponential decay, or (3) a sudden flux (Fig. 5b). The constant flux represents a fixed flux (flux = total mass / total time) released over time steps of 10 min during the duration of the limnic eruption. The exponential flux follows the decay law $C(t) = C_0 \times e^{(-\lambda \times t)}$, where C_0 is the starting flux condition in kg s^{-1} at $t = 0$ s, λ is a constant equal to 0.0012 (= ln(2)/timestep), and t is the timestep (s). The sudden flux represents complete release of all available CO_2 over the first 600 s of the eruption.

5.2. Influence of input parameters on numerical modelling

To quantify the effect of the variables involved in the dispersion process we explored the influence of: (1) seasonal meteorological conditions, (2) mechanisms of CO_2 release, and (3) the duration of the
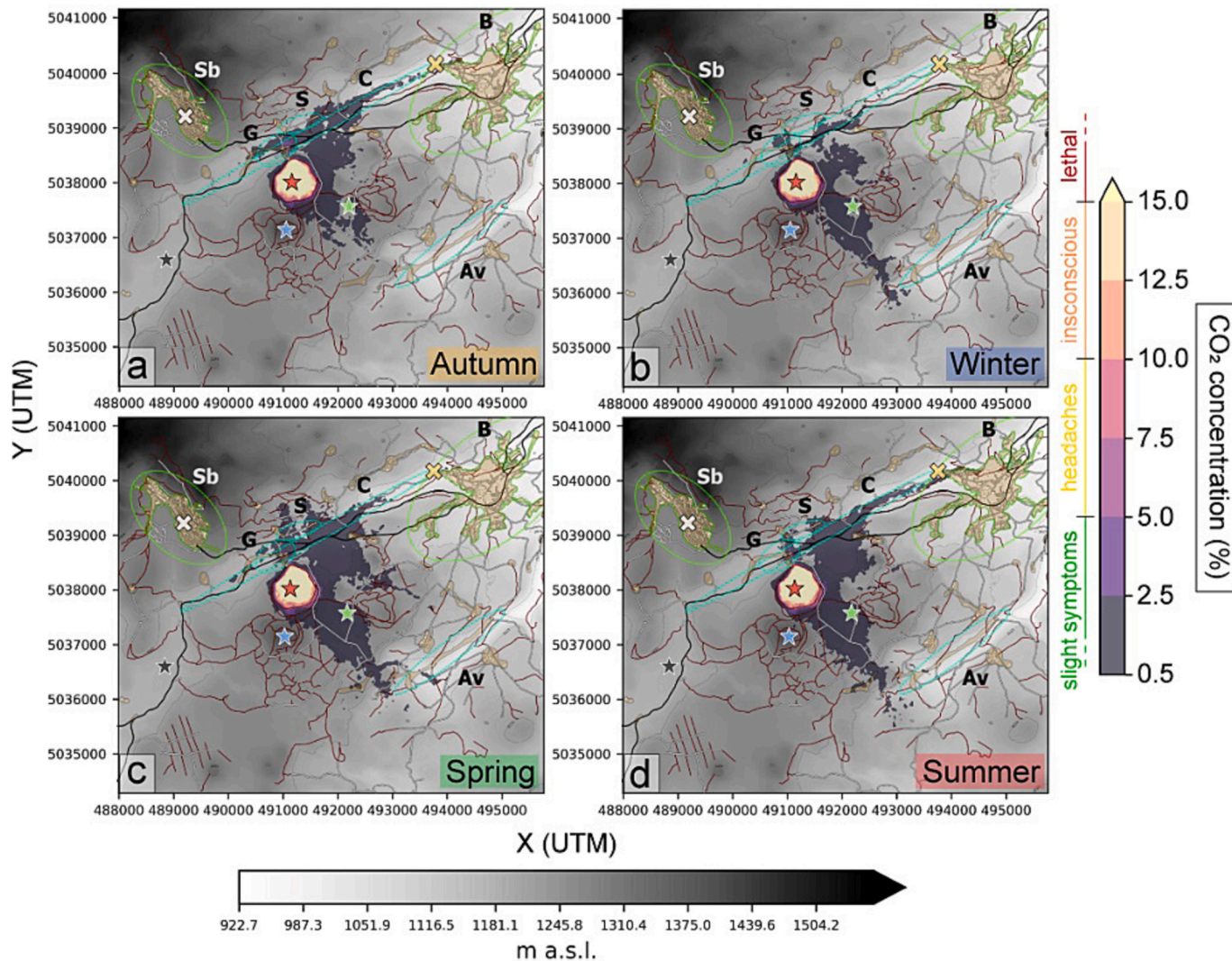
Fig. 6. Probabilistic CO_2 concentrations maps the case of a limnic eruption (*Scenario 2*) occurring in (a) autumn, (b) winter, (c) spring, and (d) summer, based on a meteorological variability of 80 days over 5 years (2016–2020) for each season. The modelling was performed at 1.50 m height from the ground, with an exceedance probability of 5%, in the case of an exponential flux with a duration of one hour. The maps represent the dispersion at t = +1 h, i.e., the end of the eruption.

limnic eruption. For these assessments we considered *Scenario 2* (limnic eruption) only, as CO_2 dispersion in the case of *Scenario 1* (current natural degassing) does not represent a hazard (excess CO_2 in the air is almost undetectable and only restricted to the area above the lake surface; Supplementary Material: Fig. S3, S4).

We first examined the influence of seasonal meteorological conditions on the CO_2 dispersion process associated with a limnic eruption (*Scenario 2*) with one-hour duration and exponential flux. Analysing the simulation results, we find that the immediate surroundings of lake Pavin are affected by the CO_2 cloud whatever the season (Fig. 6), with CO_2 content in the air at the restaurant being 13.6% in autumn and 20.7% in spring. However, the extent of the cloud varies according to season, with a maximum coverage in spring and summer, and the municipality of Besse-et-Saint-Anastaise is reached in summer (CO_2 content in the air up to 1.3% at $t = 1$ h). These results mirror the fact that spring and summer are the less windy seasons (Fig. 4), and thus favour flow of the CO_2 cloud down the Couze-Pavin valley towards Besse-et-Saint-Anastaise (Fig. 6d). As wind speed is a fundamental factor in the modelling, we focus on the two seasons that present end-member conditions: summer (lowest wind speed) and winter (highest wind speed).

We then tested the effects of the mechanism of CO_2 release on the dispersion process, with different types of fluxes. In the case of a two hour-long limnic eruption, the CO_2 cloud at $t = 2$ h remains restricted to lake Pavin (Fig. 7) for a constant CO_2 release, and for both summer and winter (Supplementary Material: Fig. S7, S8) meteorological conditions. The CO_2 content in the air is in the range 0.5–2.5% for a constant flux at the lake Pavin. In the case of an exponential flux, the CO_2 cloud spreads around the lake Pavin, and as far as the municipality of Besse-et-Saint-Anastaise, with a CO_2 content in the air exceeding 15% at the surface of the lake, and up to 19.4% at the restaurant.

Considering a one hour-long limnic eruption, CO_2 dispersion in the air at $t = 2$ h (one hour after the end of the eruption) reveals that the CO_2 cloud remains concentrated essentially at the lake (Fig. 7) in both cases: CO_2 content in the air reaches 2.5% and 10.6% at the restaurant in the case of a constant and exponential, respectively. The case of a sudden gas release (Supplementary Material: Fig. S5) is intermediate between the results obtained for the constant and exponential gas releases: the maximum extent of the CO_2 cloud is similar to the one related to an exponential gas release but the CO_2 content in the air at the lake reach 7.5% (after one hour) and 4.6% (after two hours), i.e., closer to the
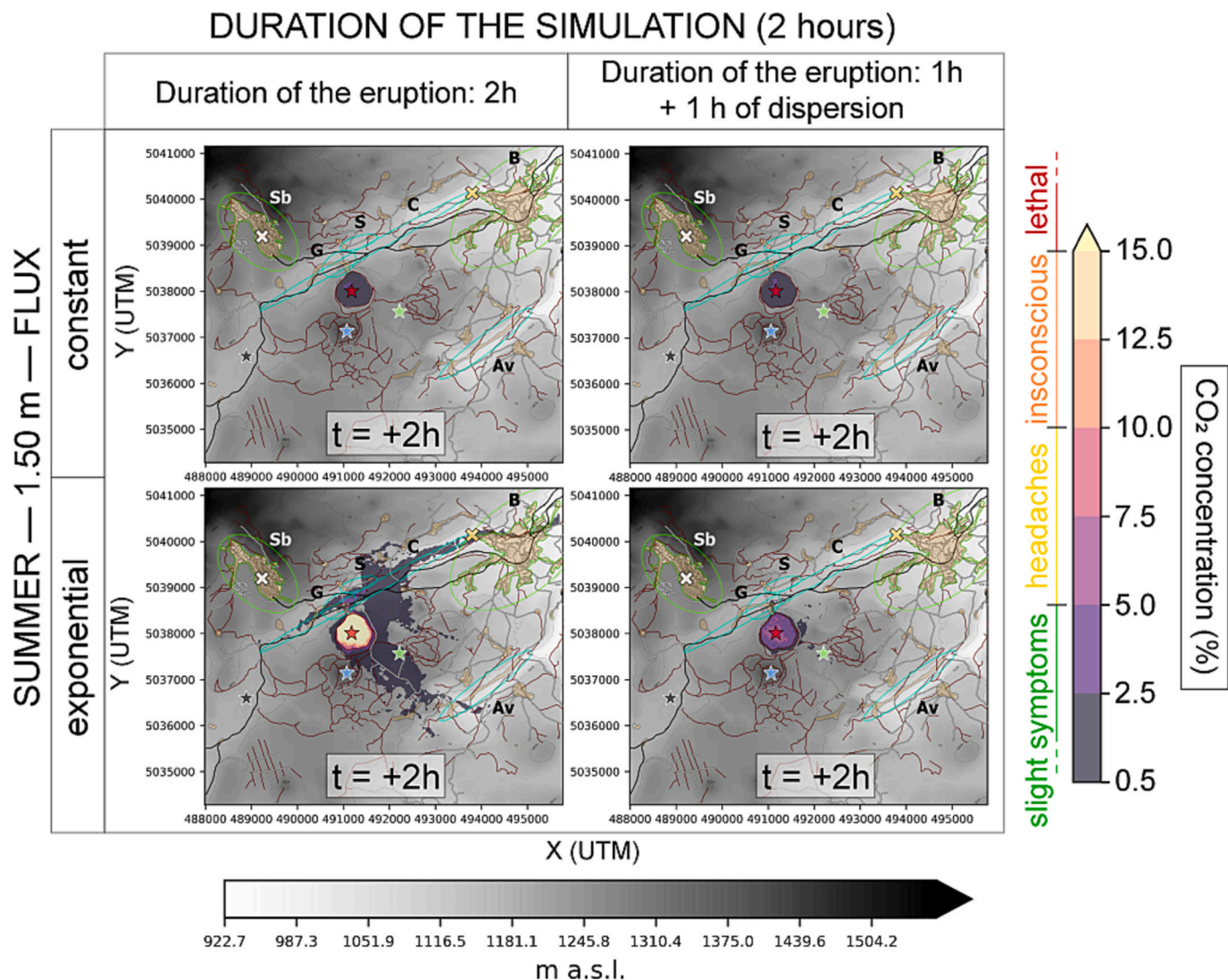

Fig. 7. Probabilistic CO_2 concentrations maps in the case of a limnic eruption (*Scenario 2*) modelled for different types of fluxes (constant and exponential) and eruption durations (first column for a two-hour eruption, second column for a one-hour eruption with one hour of dispersion). The modelling was performed at 1.50 m height from ground level in summer, with an exceedance probability of 5%. Similar results are obtained at 0.20 m height (Supplementary Material: Fig. S6) and similar conclusions are reached in the wintertime meteorological conditions (Supplementary Material: Fig. S7, S8).

values obtained for a constant gas release. Actually, in the case of a sudden gas release, the maximum CO_2 content in the air is reached at the beginning of the eruption because the following steps are triggered by the dispersion, only.

5.3. Time evolution of atmospheric CO_2 dispersion

Natural degassing at lake Pavin (*Scenario 1*) leads to maximum gas concentrations in the air that are close to the CO_2 atmospheric background (~420 ppm). Such weak increases confined to the lake surface are almost imperceptible on simulated maps whatever the season (Supplementary Material: Fig. S3, S4). The maximum excess of CO_2 in the air above the lake surface is reached in winter and reflects seasonal overturn of the mixolimnion due to thermal convection. This scenario does not pose a risk to the population and tourism at the lake Pavin.

An exponential CO_2 release during a one-hour limnic eruption at lake Pavin in summer constitutes the conditions that are likely to trigger the greatest CO_2-related risk. We thus focus on the temporal evolution of the simulations obtained in summer, where simulations obtained for the winter are available as Supplementary Material (Fig. S7, S8, S9, S10).

Release of the current dissolved CO_2 in the monimolimnion layer (*Scenario 2*) would lead to a notable increase of the CO_2 content in the air beyond the lake (Fig. 8). Ten minutes after the beginning of the limnic eruption, CO_2 remains confined to the lake but the atmospheric CO_2 concentration already exceeds 15%. After 30 min, the CO_2 cloud begins to disperse towards the north, flowing through the outlet to arrive in the Plaine du Gelat ('G' on Fig. 8). Gas dispersion towards the north is mainly related to the morphology of the maar where the low point is on the north side, where the stream outlet from the lake is located. Between 30 and 60 min after the beginning of the eruption, the cloud spreads into the Couze-Pavin valley ('C' on Fig. 8) and reaches the outskirts of Besse-et-Saint-Anastaise, where maximum CO_2 content of 1.9% is reached at t = +1 h 20 min. By the end of the eruption (t = +1 h), the CO_2 cloud has spread a little further north, reaching the hamlet of Sagnes ('S' on Fig. 8), and further south towards Estivadoux (green star on Fig. 8). Another 30 and 60 min are required for CO_2 in the air in populated areas ('B' and 'S') to decline to <0.5%. CO_2 content in the air remains at a high level at the lake level at the end of the eruption (between 12.5 and 15% at the emission point), reaching 5% at t = +2 h 30 min and only declining to <0.5% by t = +6 h.

In *Scenario 3* we consider the release of 1750 tons of dissolved CO_2 from the monimolimnion. This scenario leads to a much more widespread and rapid dispersion (Fig. 9). The same populated areas are reached by the cloud ("S", "G", and "B" on Fig. 9), but <30 min after the beginning of the eruption and with a higher content of CO_2 in the air (>15% at the Plaine du Gelat and up to 5% at Besse-et-Saint-Anastaise at t = +1 h 10 min). The CO_2 content in the air returns to <0.5% 60–90 min after the end of the eruption (compared with 30–60 min for *Scenario 2*). The cloud also does not stop at the edge of Besse-et-Saint-Anastaise but traverses the town flowing down the Couze-Pavin valley (Fig. 9). At the end of the eruption (t = +1 h), the cloud has spread over the largest area of all scenarios, reaching the populated Anglard-Vaucoux valley ('Av' on Fig. 9) and spreading upstream of the Couze-Pavin valley ('C'). At the lake, a CO_2 maximum of 52.5% is reached, and 7 h are required for levels to decrease to <0.5%.
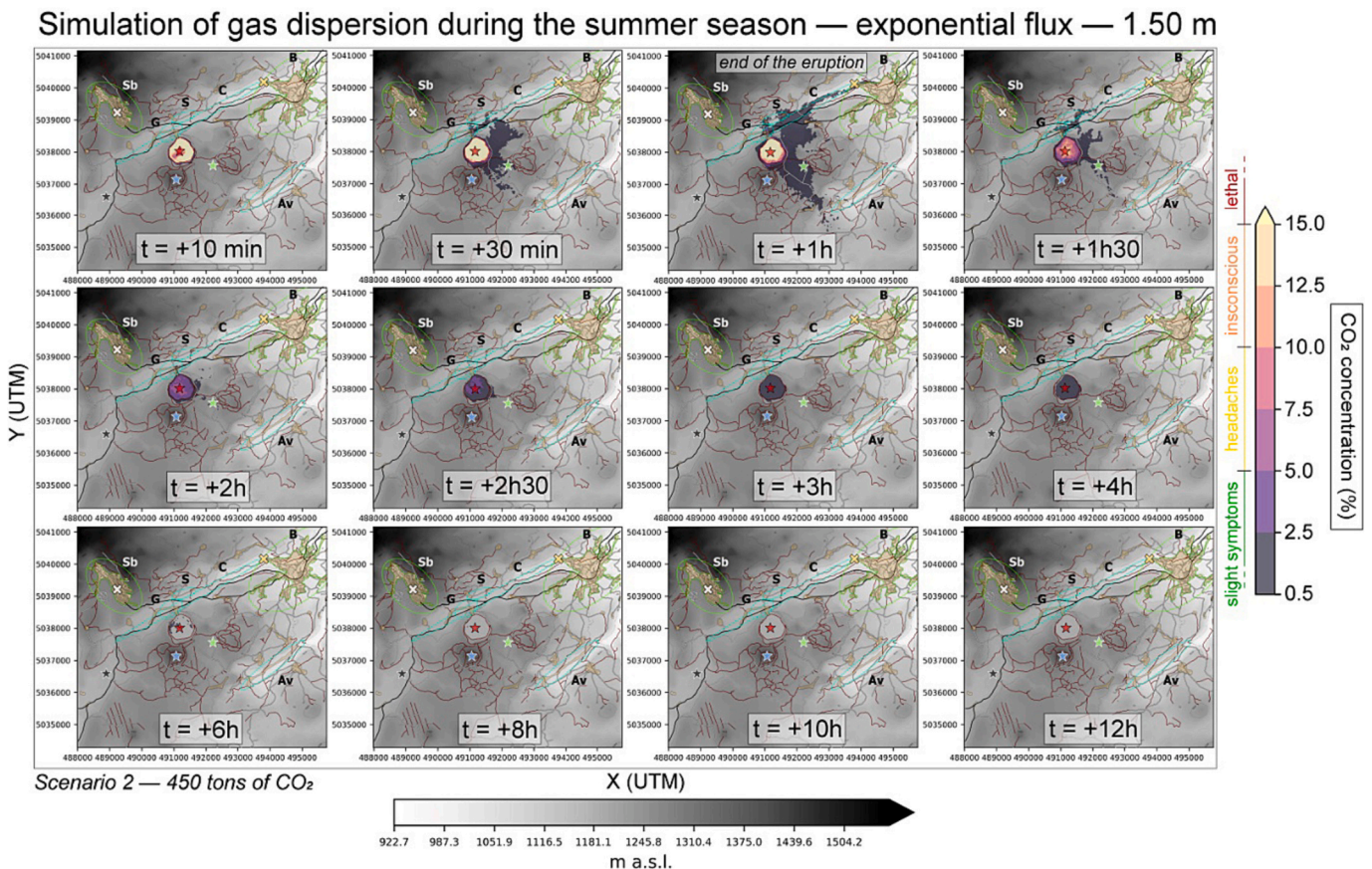

Fig. 8. Timesteps of the probabilistic simulated CO_2 content in the air in the case of a limnic eruption at the lake Pavin in summer (*Scenario 2*: 450 tons of CO_2 released) with the following parameters: 1.50 m height from ground level, exceedance probability = 5%, eruption duration = 1 h, exponential flux, and 12 h of dispersion.
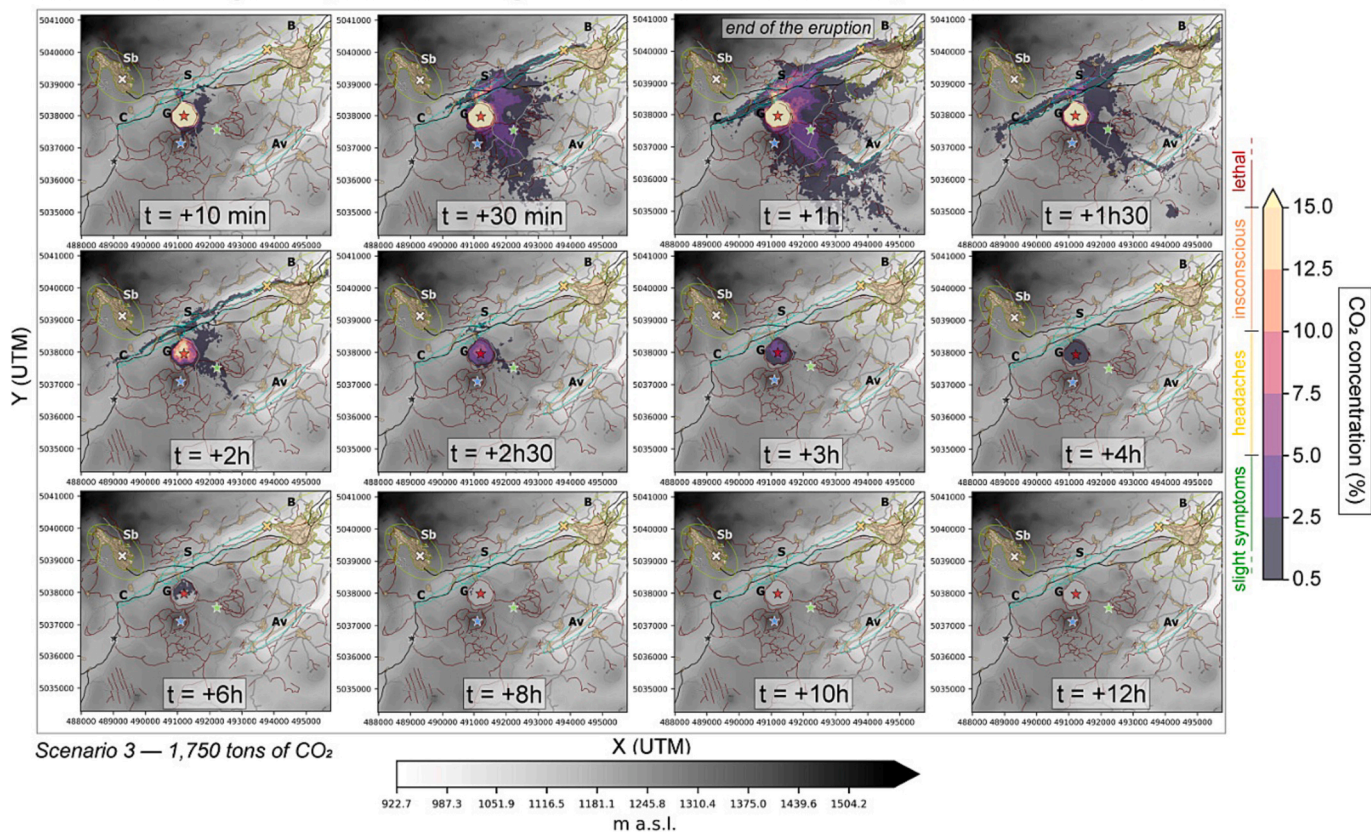
Fig. 9. Timesteps of the probabilistic simulated CO₂ content in the air in the case of a limnic eruption at lake Pavin in summer (*Scenario 3*: 1750 tons of CO₂ released) with the following parameters: 1.50 m height from ground level, exceedance probability = 5%, eruption duration = 1 h, exponential flux, and 12 h of dispersion.

5.4. Risks to human health

Limnic eruptions around the lakes of Monoun and Nyos led to around 40 and 1700 fatalities, respectively (Faivre Pierret et al., 1992; Kling et al., 1987; Kusakabe et al., 2000, 1989; Sigurdsson et al., 1987; Folch et al., 2017). In the case of a potential limnic eruption at lake Pavin, the current body of CO₂ stored in the lake (450 tons) is significantly below the that involved at lake Nyos (about 4 Mt. in January 2011; Halbwachs et al., 2020; Kusakabe, 2015) and Monoun (about 17 kt in January 2011; Kusakabe, 2015). Nevertheless, our study highlights that under some conditions (summer season and exponential flux), densely populated areas (i.e., the municipality of Besse-et-Saint-Anastaise), 3 km from lake Pavin, may be reached by the CO₂ cloud. It is thus fundamental to identify zones high-risk in respect to human health thresholds of CO₂ concentrations in the air. A short exposure to atmospheric CO₂ contents exceeding 5% starts to have harmful effects on health (https://www.cdc.gov/niosh/docs/76-194/; https://www.ivhhn.org/), where areas of CO₂ in the air reaching 0.5–5% are given as green areas (Fig. 10). In these areas breathing becomes laboured. At levels of 5–10% (yellow areas, Fig. 10), headaches, increased heart rate, sweating, dizziness, shortness of breath, muscular weakness, loss of mental abilities, drowsiness and ringing in the ears can occur. Then, between 10 and 15% (orange areas, Fig. 10), there will be loss of consciousness within 10–15 min, with headache, vomiting, vertigo, and respiratory distress and need oxygen rapidly. Beyond 15% (red areas, Fig. 10), we have lethal concentrations. The orange and red areas are thus the most critical for human health for exposure exceeding a few minutes.

Scenario 2 is considered as the most probable scenario for a limnic eruption. In this scenario, destabilisation of the lake could be triggered by landslides or climate warming rather than by a pH decrease under the

effect of external fluid supply (*Scenario 3*). The steep slopes surrounding the lake and unstable sediments have led to several landslide events in the past (Chapron et al., 2012, 2011; Thouret et al., 2021). In the French Massif Central, where regular seismic events are recorded (Battaglia and Douchain, 2017), earthquakes may favour the occurrence of landslides. The 1892 event has an intensity of 7 (www.sisfrance.net), with an epicentre near Issoire, 22 km from lake Pavin. A landslide triggering a *Scenario 2* event will be of major concern for tourists using the trails and facilities around the lake (Fig. 10), and a moderate concern populated areas within 3 km (Fig. 11). Note, too, that first responders arriving at the lake need to be aware of the hazard involved in rescue and recovery and need to be prepared and equipped accordingly (oxygen tanks and breathing apparatus). An overview for the entire modelled domain is available in Supplementary Material (Fig. S11).

Tracking point (TP1 on Fig. 10), located at the main entrance to the lake, shows that lethal CO₂ content in the air is exceeded 15 min after the beginning of the limnic eruption in the case of the *Scenario 2*, and maximum content (22%) is reached after 20 min. A little over two hours are required to return to below critical values (<10%; Fig. 10). In case of limnic eruption, the evacuation of the main entrance to the lake Pavin (including the restaurant) thus needs to be completed in <15 min. The closest evacuation point where the CO₂ content in the air remains below 0.5% during the limnic eruption is located immediately north-west of the lake, <300 m from the entrance to the lake (E1 on Fig. 10). The western part of the lake is subject to higher levels of CO₂ in the air (orange zone; Fig. 10) than the eastern or southern parts (yellow and green zones; Fig. 10). This is mainly due to the topography that also influences the altitude of the hiking path, which is much closer to the lake surface around the western portion. For visitors on the footpath's evacuation point E1 is not the closest safety point. For the western part
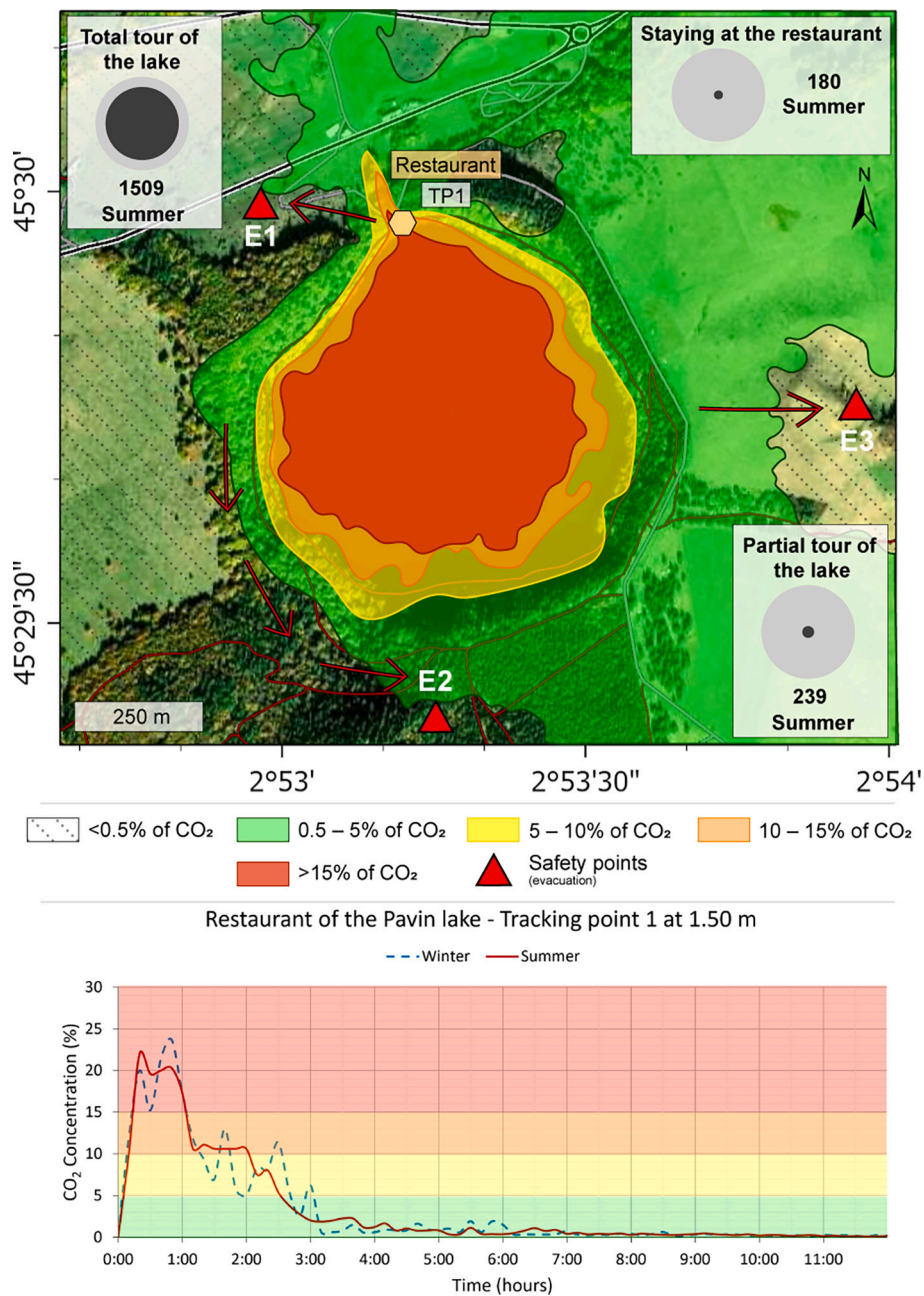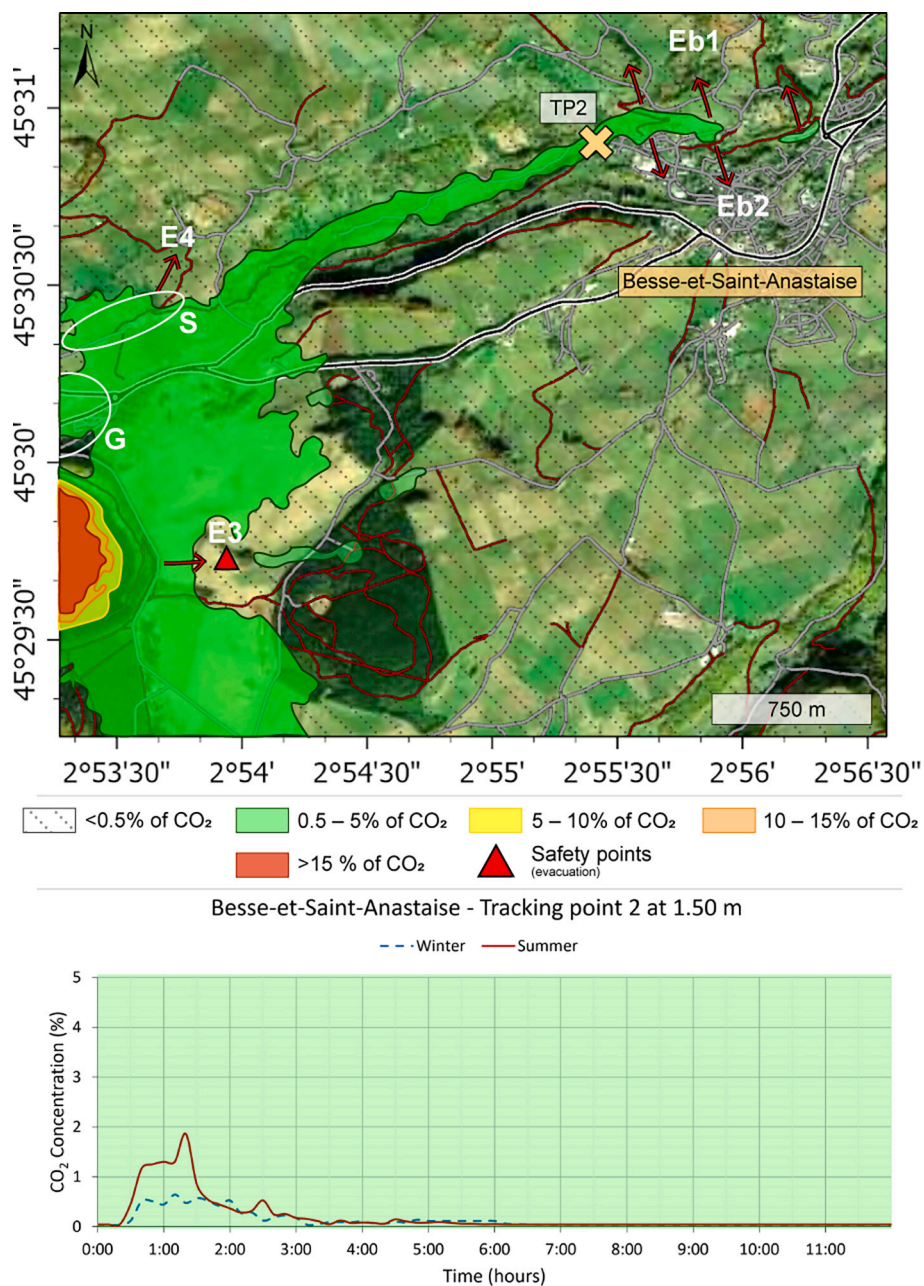
Fig. 10. Identification of risk zones (green, yellow, orange, and red) based on the simulation of a one-hour limnic eruption (*Scenario 2*) in the following conditions: height of 1.50 m from the ground, summer conditions, and exponential flux. The tourist traffic at the lake Pavin is shown for each season (see Results). The larger light-coloured circles highlight the total number of people counted at the site for the summer season (1928 people). The size of the darker inner circles is the relative number of people who either stay at the entrance (restaurant), complete the tour of the lake, or leave the main hiking path around the lake to continue on the other paths. The arrows represent the direction to reach close safety areas (little or not affected by the CO_2 cloud: E1, E2, E3). The time evolution of the CO_2 content in the air at the restaurant (tracking point TP1 – orange hexagon) is shown in the lower chart (same colour code for risk zones). (For interpretation of the references to colour in this figure legend, the reader is referred to the web version of this article.)

of the lake, safety point (E2) instead needs to be used. These areas of the lake may therefore require a prompt emergency response in the event of a limnic eruption, which could be facilitated by the installation of gas detectors, sirens and information panels, plus evacuation routing and signage (Bonilauri et al., 2021).

At Besse-et-Saint-Anastaise, tracking point TP2 (Fig. 11) represents the most exposed urban zone. Here, elevated CO_2 begin to be recorded 30 min after the beginning of the eruption. The maximum CO_2 content in the air (1.9%) is reached at t = +1 h 20 min, but never reaches critical thresholds for human health. However, it is still recommended to not be exposed to a concentration of higher than 0.5% over a continuous period

of 8 h (Boudoire et al., 2022). Thus, to avoid secondary effects such as breathing difficulties (especially for those already suffering respiratory problems) and disorientation, areas where CO_2 content remains above 0.5% for 2 h should be evacuated (Fig. 11). Inhabitants at bottom of the valley should move to safety points higher in altitude within the town (E5 and E6 on Fig. 11). A similar recommendation may be made for the inhabitants living in La Plaine du Gelat ("G") and Les Sagnes ("S") (cf. E4 on Fig. 11).

Fig. 11. Identification of risk zones (green, yellow, orange, and red) based on the simulation of a one-hour limnic eruption (*Scenario 2*) in the following conditions: height of 1.50 m from the ground, summer conditions, and exponential flux. The arrows represent the direction to reach close safety areas (little or not affected by the CO_2 cloud: E4, E5, E6). The time evolution of the CO_2 content in the air at the entrance of the municipality of Besse-et-Saint-Anastaise (tracking point TP2 – orange cross) is shown in the lower chart (same colour code for risk zones). (For interpretation of the references to colour in this figure legend, the reader is referred to the web version of this article.)

6. Conclusion

Four field campaigns were carried out at lake Pavin between May 2021 and August 2022 to (1) measure CO_2 flux at the surface of the lake, (2) estimate the budget of dissolved CO_2 contained in the lake, and (3) model the dispersion of CO_2 in the atmosphere, should it be released. Flux quantification at the lake surface, for each season, confirmed the phenomenon of water convection in the mixolimnion layer (lake overturn) at the end of autumn (2.6 tons/day) and winter (4.5 tons/day). The summertime flux is −1.2 tons/day due to photosynthetic uptake of CO_2.

By combining the flux measured at the surface with meteorological data, modelling reveals no danger to human life under current conditions. Using the estimated CO_2 budget contained in the monimolimnion, and which is available for exsolution at atmospheric pressure (450 tons of CO_2 between the depths of 80 and 92 m), we simulated the risk posed by a possible limnic eruption at lake Pavin. The probabilistic maps show that, given the current state of the lake, CO_2 content in the air for the town of Besse-et-Saint-Anastaise would increase 30 min after the beginning of the limnic eruption, reaching 2%. However, areas around the lake would experience lethal CO_2 contents in the air (>15%) <15 min after the beginning of a limnic eruption. Our work shows how hazard can be monitored, and risk assessed, at CO_2 bearing lakes.

CRediT authorship contribution statement

V. Rafflin: Writing – review & editing, Writing – original draft, Visualization, Validation, Resources, Project administration, Methodology, Investigation, Formal analysis, Data curation, Conceptualization. **G. Boudoire:** Validation, Supervision, Resources, Project administration, Investigation, Funding acquisition, Data curation, Conceptualization. **S. Massaro:** Software, Methodology. **M. Stocchi:** Software, Methodology. **A. Costa:** Software, Methodology. **F. Grassa:** Methodology, Investigation, Formal analysis. **G. Giuffrida:** Investigation. **L. Gailler:** Resources, Investigation. **M. Liuzzo:** Formal analysis. **C. Planche:** Resources. **S. Banson:** Resources. **A. Harris:** Validation, Supervision, Funding acquisition.

Declaration of competing interest

The authors declare that they have no known competing financial interests or personal relationships that could have appeared to influence the work reported in this paper.

Data availability

Data available in the supplementary material

Appendix A. Supplementary data

Supplementary data to this article can be found online at https://doi.org/10.1016/j.jvolgeores.2024.108024.

References

Aeschbach-Hertig, W., Hofer, M., Kipfer, R., Imboden, D.M., Wieler, R., 1999. Accumulation of mantle gases in a permanently stratified volcanic lake (Lac Pavin, France). Geochim. Cosmochim. Acta 63, 3357–3372. https://doi.org/10.1016/S0016-7037(99)00257-4.

Aeschbach-Hertig, W., Hofer, M., Schmid, M., Kipfer, R., Imboden, D.M., 2002. The physical structure and dynamics of a deep, meromictic crater lake (Lac The physical structure and dynamics of a deep, meromictic crater lake Lac Pavin, France). Hydrobiologia 487, 111–136. https://doi.org/10.1023/A.

Alvenerie, J., Dégot, B., Lévèque, P., Vigneaux, M., 1966. Activité en tritium et caractéristiques chimiques des eaux du Lac Pavin. C. R. Hebd. Seances Acad. Sci. 846–849 https://doi.org/10.1259/jrs.1912.0009.

Aminot, A., Kérouel, R., 2004. Hydrologie des écosystèmes marins: paramètres et analyses. Editions Quae.

Andrade, C., Viveiros, F., Cruz, J.V., Coutinho, R., 2021. Global carbon dioxide output of volcanic lakes in the *Azores archipelago*, Portugal. J. Geochem. Explor. 229, 106835 https://doi.org/10.1016/j.gexplo.2021.106835.

Anzidei, M., Carapezza, M.L., Esposito, A., Giordano, G., Lelli, M., Tarchini, L., 2008. The Albano Maar Lake high resolution bathymetry and dissolved CO_2 budget (Colli Albani volcano, Italy): constrains to hazard evaluation. J. Volcanol. Geotherm. Res. 171, 258–268. https://doi.org/10.1016/j.jvolgeores.2007.11.024.

Assayag, N., Jézéquel, D., Ader, M., Viollier, E., Michard, G., Prévot, F., Agrinier, P., 2008. Hydrological budget, carbon sources and biogeochemical processes in Lac Pavin (France): constraints from $\delta^{18}O$ of water and $\delta^{13}C$ of dissolved inorganic carbon. Appl. Geochem. 23, 2800–2816. https://doi.org/10.1016/j.apgeochem.2008.04.015.

Barberi, F., Chelini, W., Marinelli, G., Martini, M., 1989. The gas cloud of Lake Nyos (Cameroon, 1986): results of the Italian technical mission. J. Volcanol. Geotherm. Res. 39, 125–134. https://doi.org/10.1016/0377-0273(89)90053-X.

Barberi, F., Carapezza, M.L., Ranaldi, M., Tarchini, L., 2007. Gas blowout from shallow boreholes at Fiumicino (Rome): induced hazard and evidence of deep CO_2 degassing on the Tyrrhenian margin of Central Italy. J. Volcanol. Geotherm. Res. 165, 17–31. https://doi.org/10.1016/J.JVOLGEORES.2007.04.009.

Barberi, F., Carapezza, M.L., Tarchini, L., Ranaldi, M., Ricci, T., Gattuso, A., 2019. Anomalous discharge of endogenous gas at Lavinio (Rome, Italy) and the Lethal Accident of 5 September 2011. GeoHealth 3, 407–422. https://doi.org/10.1029/2019GH000211.

Battaglia, J., Douchain, J., 2017. Réseaux sismologiques d'Auvergne. Rev. Auver. 389–406.

Battani, A., Deville, E., Faure, J.L., Jeandel, E., Noirez, S., Tocqué, E., Benoît, Y., Schmitz, J., Parlouar, D., Sarda, P., Gal, F., le Pierres, K., Brach, M., Braibant, G., Beny, C., Pokryszka, Z., Charmoille, A., Bentivegna, G., Pironon, J., de Donato, P., Garnier, C., Cailteau, C., Barrès, O., Radilla, G., Bauer, A., 2010. Geochemical study of natural CO_2 emissions in the french massif central: how to predict origin, processes and evolution of CO_2 leakage. Oil Gas Sci. Technol. 65, 615–633. https://doi.org/10.2516/ogst/2009052.

Baxter, P.J., Kapila, M., Mfonfu, D., 1989. Lake Nyos disaster, Cameroon, 1986: the medical effects of large scale emission of carbon dioxide? Br. Med. J. 298, 1437–1441. https://doi.org/10.1136/bmj.298.6685.1437.

Boehrer, B., von Rohden, C., Schultze, M., 2017. Physical Features of Meromictic Lakes: Stratification and Circulation. Springer, Cham, pp. 15–34. https://doi.org/10.1007/978-3-319-49143-1_2.

Boehrer, B., Saiki, K., Ohba, T., Tanyileke, G., Rouwet, D., Kusakabe, M., 2021. Carbon dioxide in Lake Nyos, Cameroon, estimated quantitatively from sound speed measurements. Front. Earth Sci. 9, 1–8. https://doi.org/10.3389/feart.2021.645011.

Boivin, P., Besson, J.-C., Ferry, P., Gourgaud, A., Miallier, D., Thouret, J.-C., Vernet, G., 2011. Le point sur l'éruption du lac Pavin il y a 7000 ans. Rev. des Sci. Nat. Auver. 74–75, 45–55.

Bonhomme, C., Poulin, M., Vinçon-Leite, B., Saad, M., Groleau, A., Jézéquel, D., Tassin, B., 2011. Maintaining meromixis in Lake Pavin (Auvergne, France): the key role of a sublacustrine spring. C. R. Geosci. 343, 749–759. https://doi.org/10.1016/j.crte.2011.09.006.

Bonhomme, C., Jézéquel, D., Poulin, M., Saad, M., Vinçon-Leite, B., Tassin, B., 2016. Lake Pavin mixing: New insights from high resolution continuous measurements. In: Lake Pavin: History, Geology, Biogeochemistry, and Sedimentology of a Deep Meromictic Maar Lake. Springer International Publishing, pp. 177–184. https://doi.org/10.1007/978-3-319-39961-4_10.

Bonilauri, E.M., Harris, A.J.L., Morin, J., Ripepe, M., Mangione, D., Lacanna, G., Ciolli, S., Cusolito, M., Deguy, P., 2021. Tsunami evacuation times and routes to safe zones: a GIS-based approach to tsunami evacuation planning on the island of Stromboli, Italy. J. Appl. Volcanol. 10, 1–19. https://doi.org/10.1186/s13617-021-00104-9.

Boudoire, G., Finizola, A., Di Muro, A., Peltier, A., Liuzzo, M., Grassa, F., Delcher, E., Brunet, C., Boissier, P., Chaput, M., Ferrazzini, V., Gurrieri, S., 2018. Small-scale spatial variability of soil CO_2 flux: implication for monitoring strategy. J. Volcanol. Geotherm. Res. 366, 13–26. https://doi.org/10.1016/j.jvolgeores.2018.10.001.

Boudoire, G., Liuzzo, M., Cappuzzo, S., Giuffrida, G., Cosenza, P., Derrien, A., Falcone, E. E., 2020. The SoilExp software: an open-source Graphical User Interface (GUI) for post-processing spatial and temporal soil surveys. Comput. Geosci. 142, 104553 https://doi.org/10.1016/j.cageo.2020.104553.

Boudoire, G., Calabrese, S., Colacicco, A., Sordini, P., Habakaramo Macumu, P., Rafflin, V., Valade, S., Mweze, T., Kazadi Mwepu, J.C., Safari Habari, F., Amani Kahamire, T., Mumbere Mutima, Y., Ngaruye, J.C., Tuyishime, A., Tumaini Sadiki, A., Mavonga Tuluka, G., Mapendano Yalire, M., Kets, E.D., Grassa, F., D'Alessandro, W., Caliro, S., Rufino, F., Tedesco, D., 2022. Scientific response to the 2021 eruption of Nyiragongo based on the implementation of a participatory monitoring system. Sci. Rep. 12, 1–11. https://doi.org/10.1038/s41598-022-11149-0.

Boudoire, G., Pasdeloup, G., Schiavi, F., Cluzel, N., Rafflin, V., Grassa, F., Giuffrida, G., Liuzzo, M., Harris, A., Laporte, D., Rizzo, A.L., 2023. Magma storage and degassing beneath the youngest volcanoes of the Massif Central (France): lessons for the monitoring of a dormant volcanic province. Chem. Geol. 634, 121603 https://doi.org/10.1016/j.chemgeo.2023.121603.

Boyd, C.E., 2000. pH, carbon dioxide, and alkalinity. In: Water Quality. Springer, Boston, MA, pp. 105–122. https://doi.org/10.1007/978-1-4615-4485-2_7.

Bräuer, K., Kämpf, H., Niedermann, S., Wetzel, H.U., 2017. Regional distribution pattern of carbon and helium isotopes from different volcanic fields in the French Massif Central: evidence for active mantle degassing and water transport. Chem. Geol. 469, 4–18. https://doi.org/10.1016/j.chemgeo.2017.04.004.

Britter, R., McQuaid, J., 1988. Workbook on the Dispersion of Dense Gases. Tech. rep., HSE Contract Research Report No. 17/1988, Trinity Road Bootle, Merseyside L20 3QY, U. K.

Brown, S.K., Auker, M.R., Sparks, R.S.J., 2015. Populations around holocene volcanoes and development of a population exposure index. In: Global Volcanic Hazards and Risk. Cambridge University Press, pp. 223–232. https://doi.org/10.1017/CBO9781316276273.006.

Cabassi, J., Tassi, F., Vaselli, O., Fiebig, J., Nocentini, M., Capecchiacci, F., Rouwet, D., Bicocchi, G., 2013. Biogeochemical processes involving dissolved CO_2 and CH_4 at Albano, Averno, and Monticchio meromictic volcanic lakes (Central-Southern Italy). Bull. Volcanol. 75, 1–19. https://doi.org/10.1007/s00445-012-0683-0.

Camus, G., Michard, G., Olive, P., Boivin, P., Desgranges, P., Jezequel, D., Meybeck, M., Peyrus, J.-C., Vinson, J.-M., Viollier, E., Kornprobst, J., 1993. Risques d'éruption gazeuse carbonique en Auvergne. Bull. Soc. Géol. Fr. 164, 767–781. https://doi.org/10.1088/1751-8113/44/8/085201.

Carapezza, M.L., Lelli, M., Tarchini, L., 2008. Geochemistry of the Albano and Nemi crater lakes in the volcanic district of Alban Hills (Rome, Italy). J. Volcanol. Geotherm. Res. 178, 297–304. https://doi.org/10.1016/j.jvolgeores.2008.06.031.

Carpenter, S.R., 1983. Lake geometry: Implications for production and sediment accretion rates. J. Theor. Biol. 105, 273–286. https://doi.org/10.1016/S0022-5193(83)80008-3.

Caudron, C., Ohba, T., Capaccioni, B., 2017. Geochemistry and geophysics of active volcanic lakes: an introduction. Geol. Soc. Spec. Publ. 437, 1–8. https://doi.org/10.1144/SP437.18.

Chapron, E., Albéric, P., Jézéquel, D., Versteeg, W., Bourdier, J.L., Sitbon, J., 2010. Multidisciplinary characterisation of sedimentary processes in a recent maar lake (Lake Pavin, French Massif Central) and implication for natural hazards. Nat. Hazards Earth Syst. Sci. 10, 1815–1827. https://doi.org/10.5194/nhess-10-1815-2010.

Chapron, E., Alberic, P., Jézéquel, D., Ledoux, G., Massault, M., 2011. The sedimentary records of lake Pavin history. Rev. Sci. Nat. Auver. 74–75, 57–66.

Chapron, E., Ledoux, G., Simonneau, A., Albéric, P., St-Onge, G., Lajeunesse, P., Boivin, P., Desmet, M., 2012. New evidence of holocene mass wasting events in recent volcanic lakes from the french massif central (lakes pavin, montcineyre and chauvet) and implications for natural hazards. In: Submar. Mass Movements their Consequences - 5th Int. Symp., pp. 255–264. https://doi.org/10.1007/978-94-007-2162-3_23.

Chiodini, G., Cioni, R., Guidi, M., Raco, B., Marini, L., 1998. Soil CO_2 flux measurements in volcanic and geothermal areas. Appl. Geochem. 13, 543–552. https://doi.org/10.1016/S0883-2927(97)00076-0.

Chiodini, G., Granieri, D., Avino, R., Caliro, S., Costa, A., Minopoli, C., Vilardo, G., 2010. Non-volcanic CO_2 Earth degassing: case of Mefite d'Ansanto (southern Apennines), Italy. Geophys. Res. Lett. 37 https://doi.org/10.1029/2010GL042858.

Chiodini, G., Tassi, F., Caliro, S., Chiarabba, C., Vaselli, O., Rouwet, D., 2012. Time-dependent CO_2 variations in Lake Albano associated with seismic activity. Bull. Volcanol. 74, 861–871. https://doi.org/10.1007/s00445-011-0573-x.

Colella, G., 2005. Meteorologia Aeronautica, Ecologia e ambiente.

Cortis, A., Oldenburg, C.M., 2009. Short-range atmospheric dispersion of carbon dioxide. Bound. Layer Meteor. 133, 17–34. https://doi.org/10.1007/s10546-009-9418-y.

Costa, A., Chiodini, G., 2015. Modelling Air Dispersion of CO_2 from Limnic Eruptions, in: Volcanic Lakes. Springer, Berlin Heidelberg, pp. 451–465. https://doi.org/10.1007/978-3-642-36833-2_20.

Costa, A., Macedonio, G., 2016. DISGAS-2.0: A Model for Passive DISpersion of GAS. Rapp. Tec. INGV.

Costa, A., Macedonio, G., Chiodini, G., 2005. Numerical model of gas dispersion emitted from volcanic sources. Ann. Geophys. 48, 805–815.

Costa, A., Folch, A., Macedonio, G., 2013. Density-driven transport in the umbrella region of volcanic clouds: Implications for tephra dispersion models. Geophys. Res. Lett. 40, 4823–4827. https://doi.org/10.1002/GRL.50942.

Delebecque, A., 1898. Atlas des lacs français. Chamerot et Renouard.

Dioguardi, F., Massaro, S., Chiodini, G., Costa, A., Folch, A., Macedonio, G., Sandri, L., Selva, J., Tamburello, G., 2022. VIGIL: a Python tool for automatized probabilistic VolcanIc Gas dIspersion modeLling. Ann. Geophys. 65 https://doi.org/10.4401/ag-8796.

Doney, S.C., Fabry, V.J., Feely, R.A., Kleypas, J.A., 2009. Ocean acidification: The other CO2 problem. Annu. Rev. Mar. Sci. https://doi.org/10.1146/annurev.marine.010908.163834.

User's Manual for the Diagnostic Wind Model, Environ. Protect, 1990. Agency, San Rafael, Calif.

Dussart, B., 1966. Limnologie: L'étude des eaux continentales. In: Paris Gauthier-Villars. Persée - Portail des revues scientifiques en SHS..

Faivre Pierret, R.X., Berne, P., Roussel, C., Le Guern, F., 1992. The Lake Nyos disaster: model calculations for the flow of carbon dioxide. J. Volcanol. Geotherm. Res. 51, 161–170. https://doi.org/10.1016/0377-0273(92)90066-M.

Folch, A., Costa, A., Hankin, R.K.S., 2009. twodee-2: a shallow layer model for dense gas dispersion on complex topography. Comput. Geosci. 35, 667–674. https://doi.org/10.1016/j.cageo.2007.12.017.

Folch, A., Barcons, J., Kozono, T., Costa, A., 2017. High-resolution modelling of atmospheric dispersion of dense gas using TWODEE-2.1: application to the 1986 Lake Nyos limnic eruption. Nat. Hazards Earth Syst. Sci. 17, 861–879. https://doi.org/10.5194/nhess-17-861-2017.

Freeth, S.J., 1990. Lake Bambuluwe: could it be the source for a third gas disaster in western Cameroon? J. Volcanol. Geotherm. Res. 42, 393–395. https://doi.org/10.1016/0377-0273(90)90037-G.

Funiciello, R., Giordano, G., De Rita, D., 2003. The Albano maar lake (Colli Albani Volcano, Italy): recent volcanic activity and evidence of pre-Roman Age catastrophic

lahar events. J. Volcanol. Geotherm. Res. 123, 43–61. https://doi.org/10.1016/S0377-0273(03)00027-1.

Gal, F., Michel, B., Gilles, B., Frédéric, J., Karine, M., 2011. CO_2 escapes in the Laacher See region, East Eifel, Germany: application of natural analogue onshore and offshore geochemical monitoring. Int. J. Greenh. Gas Control 5, 1099–1118. https://doi.org/10.1016/j.ijggc.2011.04.004.

Gal, F., Leconte, S., Gadalia, A., 2018. The "Escarot" gas seep, French Massif Central: CO_2 discharge from a quiescent volcanic system – characterization and quantification of gas emissions. J. Volcanol. Geotherm. Res. 353, 68–82. https://doi.org/10.1016/j.jvolgeores.2018.01.026.

Giggenbach, W.F., Sano, Y., Schmincke, H.U., 1991. CO_2-rich gases from Lakes Nyos and Monoun, Cameroon; Laacher See, Germany; Dieng, Indonesia, and Mt. Gambier, Australia-variations on a common theme. J. Volcanol. Geotherm. Res. 45, 311–323. https://doi.org/10.1016/0377-0273(91)90065-8.

Glangeaud, P., 1916. Le cratère-lac Pavin et le volcan de Montchalm (Puy-de-Dôme). C. R. 'Acad. Sci. Paris 428–430.

Goepel, A., Lonschinski, M., Viereck, L., Büchel, G., Kukowski, N., 2015. Volcano-tectonic structures and CO2-degassing patterns in the Laacher See basin, Germany. Int. J. Earth Sci. 104, 1483–1495. https://doi.org/10.1007/s00531-014-1133-3.

Granieri, D., Costa, A., Macedonio, G., Bisson, M., Chiodini, G., 2013. Carbon dioxide in the urban area of Naples: contribution and effects of the volcanic source. J. Volcanol. Geotherm. Res. 260, 52–61. https://doi.org/10.1016/j.jvolgeores.2013.05.003.

Granieri, D., Carapezza, M.L., Barberi, F., Ranaldi, M., Ricci, T., Tarchini, L., 2014. Atmospheric dispersion of natural carbon dioxide emissions on Vulcano Island, Italy. J. Geophys. Res. Solid Earth 119, 5398–5413. https://doi.org/10.1002/2013JB010688.

Halbwachs, M., Sabroux, J.C., Kayser, G., 2020. Final step of the 32-year Lake Nyos degassing adventure: natural CO_2 recharge is to be balanced by discharge through the degassing pipes. J. Afr. Earth Sci. 167, 103575 https://doi.org/10.1016/j.jafrearsci.2019.103575.

Hankin, R.K.S., Britter, R.E., 1999a. TWODEE: the Health and Safety Laboratory's shallow layer model for heavy gas dispersion. Part 2: Outline and validation of the computational scheme. J. Hazard. Mater. 66, 227–237. https://doi.org/10.1016/S0304-3894(98)00275-1.

Hankin, R.K.S., Britter, R.E., 1999b. TWODEE: the Health and Safety Laboratory's shallow layer model for heavy gas dispersion. Part 1. Mathematical basis and physical assumptions. J. Hazard. Mater. 66, 211–226. https://doi.org/10.1016/S0304-3894(98)00269-6.

Hankin, R.K.S., Britter, R.E., 1999c. TWODEE: the Health and Safety Laboratory's shallow layer model for heavy gas dispersion. Part 3: Experimental validation (Thorney Island). J. Hazard. Mater. 66, 239–261. https://doi.org/10.1016/S0304-3894(98)00270-2.

Hersbach, H., Bell, B., Berrisford, P., Hirahara, S., Horányi, A., Muñoz-Sabater, J., Nicolas, J., Peubey, C., Radu, R., Schepers, D., Simmons, A., Soci, C., Abdalla, S., Abellan, X., Balsamo, G., Bechtold, P., Biavati, G., Bidlot, J., Bonavita, M., De Chiara, G., Dahlgren, P., Dee, D., Diamantakis, M., Dragani, R., Flemming, J., Forbes, R., Fuentes, M., Geer, A., Haimberger, L., Healy, S., Hogan, R.J., Hólm, E., Janisková, M., Keeley, S., Laloyaux, P., Lopez, P., Lupu, C., Radnoti, G., de Rosnay, P., Rozum, I., Vamborg, F., Villaume, S., Thépaut, J.N., 2020. The ERA5 global reanalysis. Q. J. R. Meteorol. Soc. 146, 1999–2049. https://doi.org/10.1002/QJ.3803.

Jézéquel, D., Michard, G., Viollier, E., Prévot, F., Groleau, A., Sarazin, G., Lopes, F., 2011. Carbon cycle and gas outburst hazards in the lake Pavin. Rev. Sci. Nat. Auver. 74–75, 91–110.

Jézéquel, D., Michard, G., Viollier, E., Agrinier, P., Albéric, P., Lopes, F., Abril, G., Bergonzini, L., 2016. Carbon cycle in a meromictic crater lake: Lake Pavin, France. In: Lake Pavin: History, Geology, Biogeochemistry, and Sedimentology of a Deep Meromictic Maar Lake. Springer International Publishing, pp. 185–203. https://doi.org/10.1007/978-3-319-39961-4_11.

Joanny, P., 1986. De l'eau qui sent (parfois) le soufre. La Mont.

Joanny, P., 1987. Un pharmacien clermontois raconte un souvenir de jeunesse. Le Républicain Lorrain, Interview de J. Gandebeuf.

Jouve, G., Caudron, C., Matte, G., 2021. Gas detection and quantification using iXblue Echoes high-resolution sub-bottom profiler and Seapix 3D multibeam echosounder from the Laacher See (Eifel, Germany). In: Oceans Conference Record (IEEE). Institute of Electrical and Electronics Engineers Inc. https://doi.org/10.23919/OCEANS44145.2021.9705839

Juvigné, E., Miallier, D., 2016. Distribution, tephrostratigraphy and chronostratigraphy of the widespread eruptive products of Pavin Volcano. In: Lake Pavin: History, Geology, Biogeochemistry, and Sedimentology of a Deep Meromictic Maar Lake. Springer International Publishing, pp. 143–154. https://doi.org/10.1007/978-3-319-39961-4_8.

Kling, G.W., Clark, M.A., Compton, H.R., Devine, J.D., Evans, W.C., Humphrey, A.M., Koenigsberg, E.J., Lockwood, J.P., Tuttle, M.L., Wagner, G.N., 1987. The 1986 Lake Nyos gas disaster in Cameroon, West Africa. Science (80-.). https://doi.org/10.1126/science.236.4798.169.

Kozono, T., Kusakabe, M., Yoshida, Y., Ntchantcho, R., Ohba, T., Tanyileke, G., Hell, J.V., 2017. Numerical assessment of the potential for future limnic eruptions at lakes Nyos and Monoun, Cameroon, based on regular monitoring data. Geol. Soc. Spec. Publ. 437, 163–175. https://doi.org/10.1144/SP437.8.

Kusakabe, M., 2015. Evolution of CO2 Content in Lakes Nyos and Monoun, and Sub-lacustrine CO2-Recharge System at Lake Nyos as Envisaged from $CO_2/^3He$ Ratios and Noble Gas Signatures. In: Advances in Volcanology. Springer Science and Business Media Deutschland GmbH, pp. 427–450. https://doi.org/10.1007/978-3-642-36833-2_19.

Kusakabe, M., Ohsumi, T., Aramaki, S., 1989. The Lake Nyos gas disaster: chemical and isotopic evidence in waters and dissolved gases from three Cameroonian crater lakes, Nyos, Monoun and Wum. J. Volcanol. Geotherm. Res. 39, 167–185. https://doi.org/10.1016/0377-0273(89)90056-5.

Kusakabe, M., Tanyileke, G.Z., McCord, S.A., Schladow, S.G., 2000. Recent pH and CO_2 profiles at Lakes Nyos and Monoun, Cameroon: implications for the degassing strategy and its numerical simulation. J. Volcanol. Geotherm. Res. 97, 241–260. https://doi.org/10.1016/S0377-0273(99)00170-5.

Legrand d'Aussy, P.J.-B., 1788. (1737-1800). A. du texte. In: Voyage d'Auvergne, par M. Le Grand d'Aussy. Eugène Onfroy, Librairie Quai des Augustins.

Lehman, J.T., 1975. Reconstructing the rate of accumulation of lake sediment: the effect of sediment focusing. Quat. Res. 5, 541–550. https://doi.org/10.1016/0033-5894(75)90015-0.

Leyrit, H., Zylberman, W., Lutz, P., Jaillard, A., Lavina, P., 2016. Characterization of phreatomagmatic deposits from the eruption of the Pavin Maar (France). In: Lake Pavin: History, Geology, Biogeochemistry, and Sedimentology of a Deep Meromictic Maar Lake. Springer International Publishing, pp. 105–128. https://doi.org/10.1007/978-3-319-39961-4_6.

Lide, D.R., 2003. CRC Handbook of Chemistry and Physics, 84th edn. CRC Press, Boca Raton, Florida.

Lopes, F., Viollier, E., Thiam, A., Michard, G., Abril, G., Groleau, A., Prévot, F., Carrias, J. F., Albéric, P., Jézéquel, D., 2011. Biogeochemical modelling of anaerobic vs. aerobic methane oxidation in a meromictic crater lake (Lake Pavin, France). Appl. Geochem. 26, 1919–1932. https://doi.org/10.1016/j.apgeochem.2011.06.021.

Mackay, D., Shiu, W.Y., Ma, K.C., 2000. Henry's law constant. In: Handb. Prop. Estim. Methods Chem. Environ. Heal. Sci., pp. 69–87. https://doi.org/10.1515/ci-2020-0117.

Martini, M., Giannini, L., Prati, F., Tassi, F., Capaccioni, B., Iozzelli, P., 1994. Chemical characters of crater lakes in the Azores and Italy: the anomaly of Lake Albano. Geochem. J. 28, 173–184. https://doi.org/10.2343/geochemj.28.173.

Massaro, S., Dioguardi, F., Sandri, L., Tamburello, G., Selva, J., Moune, S., Jessop, D.E., Moretti, R., Komorowski, J.C., Costa, A., 2021. Testing gas dispersion modelling: a case study at La Soufrière volcano (Guadeloupe, Lesser Antilles). J. Volcanol. Geotherm. Res. 417, 107312 https://doi.org/10.1016/j.jvolgeores.2021.107312.

Massaro, S., Stocchi, M., Tamburello, G., Costa, A., Sandri, L., Caliro, S., Chiodini, G., Selva, J., Dioguardi, F., Folch, A., Macedonio, G., 2022. Validating gas dispersion modelling at La Solfatara (Campi Flegrei, South Italy). Nuovo Cim. Soc. Ital. Fis. C 45 https://doi.org/10.1393/ncc/i2022-22186-4.

Mazot, A., Rouwet, D., Taran, Y., Inguaggiato, S., Varley, N., 2011. CO_2 and He degassing at El Chichón volcano, Chiapas, Mexico: Gas flux, origin and relationship with local and regional tectonics. Bull. Volcanol. 73, 423–441. https://doi.org/10.1007/s00445-010-0443-y.

Mazot, A., Schwandner, F.M., Christenson, B., De Ronde, C.E.J., Inguaggiato, S., Scott, B., Graham, D., Britten, K., Keeman, J., Tan, K., 2014. CO_2 discharge from the bottom of volcanic Lake Rotomahana, New Zealand. Geochem. Geophys. Geosyst. 15, 577–588. https://doi.org/10.1002/2013GC004945.

Meybeck, M., 2011. The lake pavin and its neighbours, history of an unique european heritage. Rev. Sci. Nat. Auver. 74–75, 7–44.

Meybeck, M., 2016a. Pavin, the birthplace of French limnology (1770–2012), and its degassing controversy (1986–2016). In: Lake Pavin: History, Geology, Biogeochemistry, and Sedimentology of a Deep Meromictic Maar Lake. Springer International Publishing, pp. 3–27. https://doi.org/10.1007/978-3-319-39961-4_1.

Meybeck, M., 2016b. Pavin, a rich but fragmented history (200 AD-2016). In: Lake Pavin: History, Geology, Biogeochemistry, and Sedimentology of a Deep Meromictic Maar Lake. Springer International Publishing, pp. 29–52. https://doi.org/10.1007/978-3-319-39961-4_2.

Michard, G., Viollier, E., Jézéquel, D., Sarazin, G., 1994. Geochemical study of a crater Lake: Pavin Lake, France - Identification, location and quantification of the chemical reactions in the lake. Chem. Geol. 115, 103–115. https://doi.org/10.1016/0009-2541(94)90147-3.

Millero, F.J., Pierrot, D., 1998. A chemical equilibrium model for natural waters. Aquat. Geochem. 4, 153–199. https://doi.org/10.1023/A:1009656023546.

Olive, P., Boulègue, J., 2004. Étude biogéochimique d'un lac méromictique: le lac Pavin, France / Biogeochemical study of a meromictic lake: Pavin lake, France. Géomorphol. Reli. Process. Environ. 10, 305–316. https://doi.org/10.3406/morfo.2004.1226.

Olivier, L., 1952. Sur la présence en été, dans le lac Pavin, d'une couche dépourvue d'oxygène vers 70 m de profondeur. COMPTES RENDUS Hebd. Seanc. L Acad. Sci. 234, 743–745.

Pelletier, J., 1963. Température et oxygène dissous dans la couche profonde du lac Pavin. In: Comptes Rendus 88ème Congrès Sociétés Savantes, Vol. 2, pp. 653–658.

Pelletier, J.P., 1968. Un lac meromictique, le Pavin (Auvergne). Ann. Stn. Biol. Besse-en-Chandesse 147–170.

Pfanz, H., Saßmannshausen, F., Wittmann, C., Pfanz, B., Thomalla, A., 2019. Mofette Vegetation as an Indicator for Geogenic CO_2 Emission: a Case Study on the Banks of the Laacher See Volcano, Vulkaneifel, Germany. Geofluids 2019. https://doi.org/10.1155/2019/9589306.

Planche, C., Wobrock, W., Flossmann, A.I., Tridon, F., Labbouz, L., Van Baelen, J., 2013. Small scale topography influence on the formation of three convective systems observed during COPS over the Vosges Mountains. Meteorol. Z. 22, 395–411. https://doi.org/10.1127/0941-2948/2013/0402.

Roe, G.H., O'Neal, M.A., 2009. The response of glaciers to intrinsic climate variability: observations and models of late-Holocene variations in the Pacific Northwest. J. Glaciol. 55, 839–854. https://doi.org/10.3189/002214309790152438.

Rouwet, D., Tassi, F., Mora-Amador, R., Sandri, L., Chiarini, V., 2014. Past, present and future of volcanic lake monitoring. J. Volcanol. Geotherm. Res. 272, 78–97. https://doi.org/10.1016/j.jvolgeores.2013.12.009.

Rouwet, D., Chiodini, G., Ciuccarelli, C., Comastri, A., Costa, A., 2019. Lago Albano, the "anti-Nyos-type" lake: the past as a key for the future. J. Afr. Earth Sci. 150, 425–440. https://doi.org/10.1016/j.jafrearsci.2018.09.019.

Rouwet, D., Tamburello, G., Chiodini, G., Pecoraino, G., Procesi, M., Ricci, T., Venturi, S., Santi, A., Cabassi, J., Vaselli, O., Tassi, F., Costa, A., 2020. New insights into the degassing dynamics of Lago Albano (Colli Albani volcano, Rome, Italy) during the last three decades (1989-2019). Ital. J. Geosci. 139, 1–13. https://doi.org/10.3301/IJG.2020.19.

Sigurdsson, H., 1988. Gas Bursts from Cameroon Crater Lakes: a New Natural Hazard. Disasters 12, 131–146. https://doi.org/10.1111/j.1467-7717.1988.tb00661.x.

Sigurdsson, H., Devine, J.D., Tchua, F.M., Presser, F.M., Pringle, M.K.W., Evans, W.C., 1987. Origin of the lethal gas burst from Lake Monoun, Cameroun. J. Volcanol. Geotherm. Res. 31, 1–16. https://doi.org/10.1016/0377-0273(87)90002-3.

Small, C., Naumann, T., 2001. The global distribution of human population and recent volcanism. Environ. Hazards 3, 93–109. https://doi.org/10.1016/S1464-2867(02)00002-5.

Talling, J.F., 2010. pH, the CO_2 system and freshwater science. Fr. Rev. 3, 133–146. https://doi.org/10.1608/frj-3.2.156.

Tazieff, H., 1989. Mechanisms of the Nyos carbon dioxide disaster and of so-called phreatic steam eruptions. J. Volcanol. Geotherm. Res. 39, 109–116. https://doi.org/10.1016/0377-0273(89)90051-6.

Thouret, J.C., Boivin, P., Miallier, D., Donnadieu, F., Dumoulin, J.P., Labazuy, P., 2021. Post-eruption evolution of maar lakes and potential instability: the Lake Pavin case study, French Massif Central. Geomorphology 382, 107663. https://doi.org/10.1016/j.geomorph.2021.107663.

Thuiller, W., 2007. Biodiversity: climate change and the ecologist. Nature. https://doi.org/10.1038/448550a.

Vaselli, O., Capaccioni, B., Tedesco, D., Tassi, F., Yalire, M., 2003. The "evil winds" (mazukus) at Nyiragongo Volcano (Democratic Republic of Congo). Acta Vulcanol. J. Natl. Volcan. Gr. Italy 14–15, 123–128.

Vaselli, O., Tedesco, D., Cuoco, E., Tassi, F., 2015. Are Limnic Eruptions in the CO_2–CH_4-Rich Gas Reservoir of Lake Kivu (Democratic Republic of the Congo and Rwanda). In: Possible? Insights from Physico-Chemical and Isotopic Data, in: Advances in Volcanology. Springer Science and Business Media Deutschland GmbH, pp. 489–505. https://doi.org/10.1007/978-3-642-36833-2_22.

Villemant, B., Caron, B., Thierry, P., Boivin, P., 2016. Magmatic evolution of Pavin's group of volcanoes: Petrology, geochemistry and modeling of differentiation processes. A preliminary study. In: Lake Pavin: History, Geology, Biogeochemistry, and Sedimentology of a Deep Meromictic Maar Lake. Springer International Publishing, pp. 129–142. https://doi.org/10.1007/978-3-319-39961-4_7.

Viollier, E., 1995. Geochimie des elements traces en milieu lacustre. http://www.theses.fr. Paris 7.

Viveiros, F., Gaspar, J.L., Ferreira, T., Silva, C., 2016. Hazardous indoor CO_2 concentrations in volcanic environments. Environ. Pollut. 214, 776–786. https://doi.org/10.1016/j.envpol.2016.04.086.

Viveiros, F., Baldoni, E., Massaro, S., Stocchi, M., Costa, A., Caliro, S., Chiodini, G., Andrade, C., 2023. Quantification of CO_2 degassing and atmospheric dispersion at Caldeiras da Ribeira Grande (São Miguel Island, Azores). J. Volcanol. Geotherm. Res. 438, 107807 https://doi.org/10.1016/j.jvolgeores.2023.107807.

Wallace, J.M., Hobbs, P.V., 2006. Atmospheric Science: An Introductory Survey: Second Edition, Atmospheric Science: An Introductory Survey, Second edition. Academic Press. https://doi.org/10.1016/C2009-0-00034-8.

Wilhelm, E., Battino, R., Wilcock, R.J., 1977. Low-pressure Solubility of gases in liquid water. Chem. Rev. 77, 219–262. https://doi.org/10.1021/cr60306a003.

Zimmer, M., Tassi, F., Vaselli, O., Kujawa, C., Cabassi, J., Erzinger, J., 2016. The gas membrane sensor (GMS) method: a new analytical approach for real-time gas concentration measurements in volcanic lakes. Geol. Soc. Spec. Publ. 437 https://doi.org/10.1144/SP437.1.